The Thesis Committee for Nicholas James Brenes
Certifies that this is the approved version of the following thesis:

Paper Analytical Devices for Rapid, Quantitative Electrochemical Detection of DNA and Bacteria

APPROVED BY
SUPERVISING COMMITTEE:

Supervisor: _____
Richard Crooks

_____
Shelley Payne

Paper Analytical Devices for Rapid, Quantitative Electrochemical Detection of DNA and Bacteria

by

Nicholas James Brenes, B.S.

Thesis

Presented to the Faculty of the Graduate School of

The University of Texas at Austin

in Partial Fulfillment

of the Requirements

for the Degree of

Master of Arts

The University of Texas at Austin

December 2016

Abstract

Paper Analytical Devices for Rapid, Quantitative Electrochemical Detection of DNA and Bacteria

Nicholas James Brenes, M.A.

The University of Texas at Austin, 2016

Supervisor: Richard Crooks

In this thesis, two paper analytical devices (PADs) are described as proof of concept devices for point-of-care applications. The first PAD, termed the Esensor, was developed for quantitative detection of oligonucleotides. The detection component of the Esensor was based on DNA stem-loop probe hybridization with signal stranded DNA followed by transduction of an electrochemical signal via target-induced conformational switching. The electrochemical signal was produced by a redox label attached to the DNA stem-loop probe. The Esensor had a limit of detection of 30 nM for DNA, and the device-to-device reproducibility was better than 10%. Furthermore, the Esensor had a shelf life of at least 4 weeks and required only 20 μL of sample.

The Esensor work presented in this thesis was published in Analytical Chemistry where the detection of DNA and thrombin was described.[1] The Esensor work was completed in collaboration with Dr. Cunningham who is the primary author on the publication. This thesis focuses only on the detection of DNA by the Esensor, as I have made significant contributions to this portion of the work.

The second PAD covered in this thesis was developed for the detection of whole-cell bacteria. The operation of the device involved a sandwich capture assay. Bacterial specificity was achieved using antibody-functionalized magnetic microbeads and silver nanoparticle (AgNP) labels. The AgNP labels allowed for electrochemical detection via anodic stripping voltammetry. In this sensor, there were two inherent forms of signal amplification: (1) magnetic concentration of microbeads complexed with bacteria at the working electrode surface and (2) electrochemical concentration of Ag^+ ions at the working electrode surface. This PAD was nearly 100% specific for *Escherichia coli* (*E. coli)* in the presence of two additional bacterial species. The on-chip assay time was <4 min, the device fabrication was cost effective at $0.36 USD/device, and the limit of detection was 1.3×10^7 cells/mL. This device, termed the oSlipB, was similar to a PAD employed to detect DNA and proteins as previously reported;[2–5] however, this new application of bacterial detection further exemplifies the versatility of this paper device.

Table of Contents

List of Figures

List of Illustrations

Chapter 1. Introduction

1.1 Properties and Uses of Paper Analytical Devices

Paper analytical devices (PADs) date back as far as the 1800s when Gay-Lussac first described the litmus paper test for acids.[6,7] Since then, the development of applications for chemistry on paper was slow but steady until the breakthrough of chromatography and separations in the 1940s.[6,7] In the 1970s the Ames company released the first battery powered glucose meter. This PAD employed a paper test strip and enzymes to determine glucose levels in blood for patients with diabetes. The next big advancement in PADs occurred in 1988 when Unipath released the home pregnancy test. This is perhaps one of the most renowned PADs developed in the past century. This PAD tests for the presence of a female pregnancy hormone using antibodies attached to a paper platform.[8] Modern era PADs trace back to 2007 and 2008, when 2- and 3-dimensional PADs were first shown to detect glucose and the protein bovine serum albumin.[9,10] Since then, there has been several leaps in PAD technologies allowing for the construction of relatively complex fluidic PADs for the detection of biological analytes and harmful environmental contaminants.

The surge in research and development of PADs over the past few years has been likely due to the many advantageous characteristics paper has over traditional sensor substrates, e.g., glass, silicon, or polymer based sensors such as PET (poly(ethylene terephthalate)).[6,7,11,12] One of paper's most attractive qualities is cost. Paper is 200 times less expensive than PET and 1,000 times less expensive than glass.[6] From a scientific standpoint, paper is a biocompatible material that has a high surface area, and paper's capillary action eliminates the need for costly pumps.[6,7,12,13] Furthermore, PADs are

easily prototyped, manufactured, and functionalized.[6,7] It is these desirable attributes that make paper based sensors ideal for rapid, point-of-care diagnostics.[6,7,11–13]

An example of an inexpensive PAD for environmental testing was presented by Chen *et al.* in 2014.[14] They developed a PAD for rapid detection of mercury (Hg^{2+}) in pond and river water. The sensor employed gold nanoparticles (AuNPs) and DNA as a means for detection. AuNPs were capped with an oligonucleotide sequence containing a thymine-thymine mismatch. In the presence of water contaminated with Hg^{2+}, the DNA oligonucleotides underwent a conformation change, forming a hairpin structure via thymine-Hg^{2+}-thymine interaction. This conformational change released the DNA cap from the AuNPs, allowing the free AuNPs to aggregate in solution. This aggregation generated a color change that was easily detected using a smart phone. This PAD was able to detect mercury concentrations as low as 50 nM in spiked pond water.[14] Furthermore, the authors' sensor demonstrates that the characteristics of PADs (wettability, disposability, simple fabrication etc.) are ideal for routine testing in the field.

In addition to environmental testing, paper based sensors may also form a pivotal role for point-of-care testing in resource-limited regions of the world.[7] For example, Malaria, caused by the parasite *Plasmodium,* affects over 106 countries worldwide.[15] In 2015, Malaria was responsible for 214 million clinical episodes and over 438,000 deaths.[15] Most of these cases were concentrated in remote areas of the world.[16] In light of epidemics like malaria, there has been a large drive to develop PADs for the detection of pathogenic diseases that employ little to no resources like electricity or clean water.[17] As a proof of concept, Fu *et al.* detected a histidine rich protein (PfHRP2) from *Plasmodium falciparum* using a 2-dimensional PAD. They employed an immuno-sandwich capture assay using antibody-functionalized AuNPs that bind the target protein with high specificity. The AuNPs acted as a colorimetric indicator for the presence of PfHRP2

protein. An increase in AuNPs concentration meant the sample was positive for the presence of the malarial protein, which was easily monitored using a scanner. Unique to this PAD was how the authors achieved washing and signal amplification. By simply adding sample and water to specific locations on the PAD and using origami, the authors achieved a multistep automated process which allowed for rehydration of reagents and washing. With a signal amplification reagent, this PAD had a limit of detection (LOD) of 2.9 $\pm$ 1.2 ng/mL of PfHRP2.[17] This LOD was slightly better than that achieved by a standard enzyme-linked immunosorbent assays (ELISA), 4 ng/mL of PfHRP2.[17] The fabrication and manufacturing of lightweight, inexpensive PADs like the one described here would allow health care workers to overcome many of the obstacles associated with disease detection in resource-limited regions of the world.

Up to this point only paper sensors using colorimetric detection have been discussed. While colorimetric detection has the advantage of little to no instrumentation, it is only semi-quantitative at best.[11,12] In order to achieve more accurate, sensitive and quantitative measurements, PADs must employ other means of detection: electrochemical transduction, fluorescence, surface enhanced Ramen spectroscopy, etc.[6,12] For example, paper based sensors that employ electrochemical detection have the advantage of speed, selectivity, and sensitivity while being insensitive to light, dust, and insoluble compounds.[6,7] Additionally, paper based sensors utilizing electrochemical detection can be easily integrated into robust, portable, miniaturized platforms allowing for straight forward digital readouts.[7] While these more complicated detection methods require instrumentation and additional resources, advancements in analytical instruments over the past few decades have made employing paper sensors in remote field testing more practical.[6] It is for these reasons we have focused on the development of PADs utilizing electrochemical detection as presented in this work.

1.2 PADs Designed by the Crooks Group

The Crooks group has contributed to the paper microfluidic field by introducing new PAD technologies: origami, slip layers, and hollow channels (Illustration 1a-c). Origami (paper folding) techniques have allowed PADs to achieve both 2- and 3-dimensional flow (Illustration 1a).[18] Additional functionality to PADs was added using a slip layer to create the SlipPAD.[19] The SlipPAD consists of two wax patterned pieces of paper that slide relative to one another (Illustration 1b). The slip layer may be employed in a variety of tasks including reagent delivery and sample washing. Lastly, the Crooks' group developed hollow channels by removing a section of paper sandwiched between two layers of wax patterned paper (Illustration 1c).[20] Hollow channels offer a number of advantages including reduced non-specific adsorption, faster flow rates, and accommodation of micron-sized objects within PADs.[20] These advancements have led to the successful development of two novel PADs, the Esensor and the oSlip. These novel sensors have been coupled with electrochemical detection methods to achieve quantitative detection of biological agents and will be the focus of this thesis.[1,2,5]

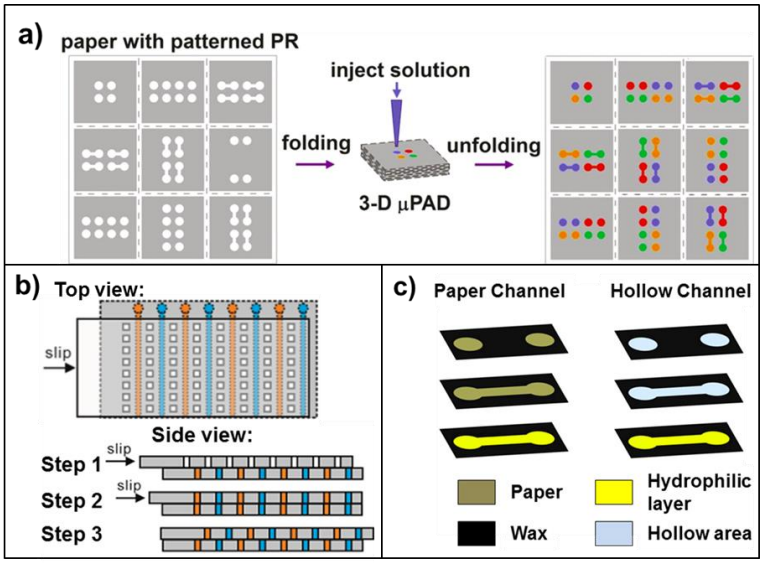

Illustration 1: Crooks Group Contributions to the Paper Microfluidic Field

a) Origami Technology. Example of 3-D flow within an origami PAD. Paper was patterned with photo resist (PR) and the dye pattern shows flow of solution once unfolded. b) Slip Layer Technology. Example of the SlipPAD delivery method. Two dyes were dispensed on the bottom layer of wax patterned paper. The top layer of paper was slid over the bottom layer to simultaneously uptake the dye demonstrating simultaneous delivery. Reprinted with permission from Ref. 19. Copyright 2013 American Chemical Society. c) Hollow Channel Technology. Three layers of stacked paper highlighting the differences between a paper channel and hollow channel. Hollow channels allow for faster flow rates and incorporation of micro-sized objects within PADs.

1.3 THESIS OVERVIEW

This thesis describes the fabrication and operation of two PADs as proof of concept devices for point-of-care applications. The focus of Chapter 2 is the development of the Esensor PAD for quantitative detection of oligonucleotides. Detection was based on DNA stem-loop probe hybridization with signal stranded DNA followed by transduction of an electrochemical signal via target-induced conformational switching. The electrochemical signal was produced by a redox label attached to the DNA stem-loop

probe. The Esensor had a LOD of 30 nM, and the device-to-device reproducibility was better than 10%. Furthermore, the Esensor has a shelf life of at least 4 weeks and required only 20 µL of sample for testing. The work presented in this thesis was published in Analytical Chemistry where the detection of DNA and thrombin using the Esensor was described.[1] This work was completed in collaboration with Dr. Cunningham, the lead scientist on the project; however, only work describing the detection of DNA is presented in this thesis, as I have significantly contributed to this portion of the work.

In Chapter 3, detection of whole-cell bacteria using a simple, origami-folded PAD employing a slip layer and hollow channels is reported. The operation of the device involves a sandwich capture assay. Bacteria were recognized by antibody-functionalized magnetic microbeads and subsequent electrochemical detection of silver nanoparticle (AgNP) labels. The sensor was nearly 100% specific for *E. coli* in the presence of additional bacterial species. The on-chip assay time was <4 min, the device was cost effective at $0.36 USD/device, and the lowest bacterial concentration detected was 1.3 x 10^7 cells/mL. This device, termed the oSlipB, was similar to a PAD employed to detect DNA and proteins as previously reported;[2–5] however, this new application of bacterial detection further demonstrates the versatility of this paper device.

Chapter 2. Paper Electrochemical Device for Detection of DNA and Thrombin by Target-Induced Conformational Switching[1]

2.1 Introduction and Background

In recent years paper based sensors have had an increasing presence in the literature for point-of-care diagnostics, food quality control, and environmental monitoring.[6,21] Many of these paper based sensors employ antibodies as biological recognition elements; however, the use of antibodies on PADs has many limitations including cost, stability, and difficulty of modification.[22] Aptamers provide a good alternative to antibodies. Aptamers are small RNA, DNA, or peptide fragments that bind molecular targets with high specificity. Like antibodies, aptamers can be selected to recognize a wide range of analytes and are easily modified or functionalized; however, unlike antibodies, aptamers are more stable for long term storage.[23] The use of aptamers as capture reagents in combination with electrochemical detection has led to a class of sensors termed electrochemical aptamer based sensors (E-AB sensors). Similarly, oligonucleotides bound to an electrode for detection of specific DNA or RNA sequences have been termed (E-DNA sensors).[24–26] Both E-AB and E-DNA sensors are sensitive, highly specific towards their target analytes (even in complex matrices), and are easily reconfigurable to detect a range of analytes. E-AB sensors have been shown to detect RNAs, proteins, small molecules, and inorganic ions.[24–26]

These sensors function by recognition of an analyte via molecular interactions with the DNA, RNA or peptide probe. The molecular interactions between target and probe generate a change in the conformation and/or flexibility of the target-probe

---

[1]Cunningham, J. C.; Brenes, N. J.; Crooks, R. M. Paper Electrochemical Device for Detection of DNA and Thrombin by Target-Induced Conformational Switching. *Anal. Chem*. **2014**, 86, 6166–6170.
I was the second author on this publication and significantly contributed to the work presented in Chapter 2.

complex that ultimately translates into a detectable signal.[24–27] Probes functionalized with redox molecules attached to an electrode transduce electrochemical signals based on the proximity of the redox molecule to the electrode.[24–27] Two types of sensors may be developed using this technique. The first type, an "on" sensor, functions by moving the redox label closer to the electrode upon target binding, resulting in an increase in electrochemical signal (Illustration 2a). The second type, an "off" sensor, functions by moving the redox label further away from the electrode upon bind the target and results in a decrease in electrochemical signal (Illustration 2b).

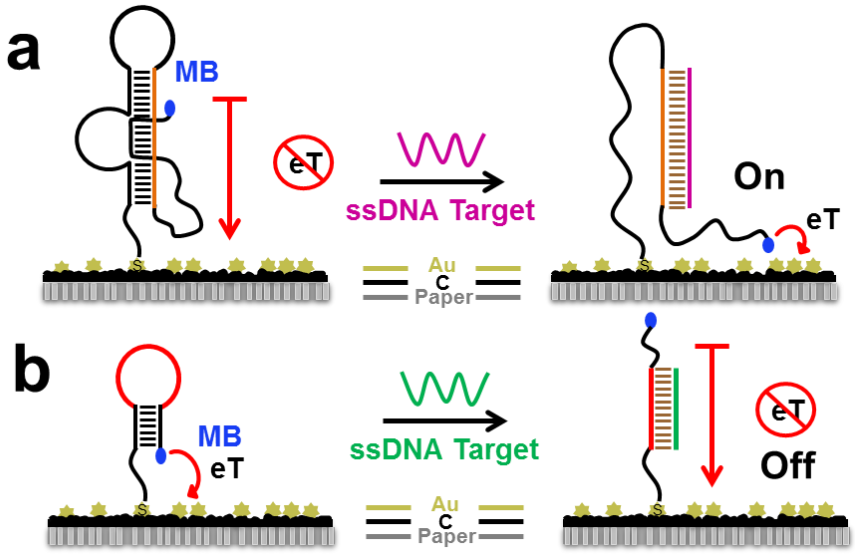

Illustration 2: Types of E-DNA Sensors

Illustration highlighting the difference between an E-DNA "on sensor" (a) and an E-DNA "off sensor" (b). In both examples, the analyte is the complementary single-stranded DNA (ssDNA) target sequence. Changes in conformation of the functionalized DNA probe occur upon binding of target DNA strand, ultimately moving the methylene blue (MB) redox label towards or away from the electrode causing changes in electron transfer efficiency. a) was adapted with permission from Ref. 27. Copyright 2009 American Chemical Society.

There have been many reports of E-DNA sensors in conventional three electrode electrochemical cells.[28–30] Plaxco and coworkers have utilized surface-bound conformational switching probes to detect various analytes including proteins,[28,31,32] antibodies,[33,34] and DNA[29,35] in various biologically relevant matrices such as blood and serum.[30,31,36–38] Other groups have also made significant contributions to these types of sensors.[39–44] Impressively, Ferguson *et al.* developed a microfluidic electrochemical device called MEDIC to monitor clinically relevant concentrations of the anti-tumor agent doxorubicin and the antibiotic kanamycin, *in vivo* and in real time.[31] The MEDIC device was a rectangular laminar flow device composed of polydimethylsiloxane, glass, and multiple gold working electrodes. The microfluidic device used E-AB probes attached to gold working electrodes as the recognition and signal transduction elements. The device functions by using simultaneous laminar flow of buffer over blood, allowing the diffusion of low molecular weight analytes through the buffer to the E-AB probes. Capture of the analyte by E-AB probes allowed the authors to determine the concentration of analyte in the blood via electron transfer efficiency. By switching the E-AB probes in the MEDIC device, the authors were able to change the specificity from reporting real time, *in vivo* concentrations of doxorubicin to reporting real time, *in vivo* concentrations of kanamycin.[31]

Inspired by Plaxco[29–31] and others[39–44], we developed a paper based E-DNA sensor (Esensor) for the detection of single stranded DNA (ssDNA) targets. The Esensor was an "off" sensor and utilized SlipPAD technology.[19] The Esensor had a LOD of 30 nM for ssDNA, and the device-to-device reproducibility was better than 10%. Furthermore, the Esensor's shelf life was at least 4 weeks and required only 20 µL of sample.

2.2 EXPERIMENTAL

2.2.1 Chemicals and Materials

$AuCl_4^-$, KNO_3, and tris (2-carboxyethyl) phosphine hydrochloride (TCEP-HCl) were purchased from Sigma-Aldrich. Whatman grade 1 chromatography paper, Tris-HCl buffer, H_2SO_4, KCl, $MgCl_2$, and NaCl were all purchased from Fisher Scientific. KH_2PO_4 was purchased from EM Science. All oligonucleotides were purchased from Biosearch Technologies. 6-mercapto-1-hexanol was purchased from Acros Organics. All chemicals were at least reagent grade. The conductive carbon ink (CI-2042) and Ag/AgCl ink (CI-4002) were purchased from Engineered Conductive Materials (Delaware, Ohio). A Xerox Color Cube 8570 printer was used to print solid wax on the chromatography paper. A CHI Model 650c (CH Instruments, Austin, TX) potentiostat was used for all experiments. All solutions were prepared using deionized water (18.0 MΩ-cm, Milli-Q Gradient System, Millipore). All reagents were used as received without further purification. Experiments were conducted at room temperature (23 ± 2 °C).

2.2.2 Esensor Device Fabrication

The Esensor contains two layers, a base layer and a slip layer (Illustration 3a). The base layer fabrication begins by printing black wax ink on both sides of Whatman 1 chromatography paper. The chromatography paper was then heated to melt the wax through the paper (120 °C, 1 min). Double-sided printing was used to increase the hydrophobicity of the paper, thereby preventing leaking during the DNA immobilization and hybridization steps discussed later. Next, conductive carbon ink was screen printed onto the chromatography paper to create three electrodes, then placed in an oven to dry (60 °C, 10 min). Afterwards, the devices were realigned and re-screen printed with the

conductive carbon ink to increase the electrodes' thickness and conductivity. The devices were placed an oven to cure (60 °C, 1 hr).

A reference electrode was created by painting Ag/AgCl ink onto one of the carbon electrodes using a fine paintbrush. The devices were cured (23 °C, 1 hr) and cut from the chromatography paper using a razor blade. A hole was punched out on the tab protruding from the bottom left side of the base layer (Illustration 3a). The function of the tab was to hold the slip layer atop the base layer as well as provide a sample application port (Illustration 3b and 3c).

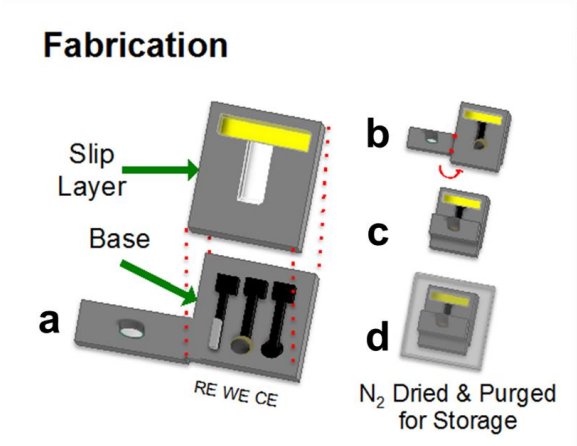

Illustration 3: Fabrication of the Esensor

a) The slip layer was stacked on top of the base layer. The three electrodes were: a Ag/AgCl reference electrode (RE), carbon paste working electrode modified with gold clusters (WE), and a carbon paste counter electrode (CE). b and c) The tab on the bottom left side of the base layer was folded over the slip layer. d) The DNA stem loop was attached to the gold electrode, dried with N_2 and stored in a laminated pouch. Illustration 3 was adapted with permission from Ref. 1. Copyright 2014 American Chemical Society.

A gold working electrode (WE) was prepared by electrochemically activating the center carbon electrode via cyclic voltammetry (0.5 M H_2SO_4, -0.2 V to 1.35 V, 0.1 V/s,

20 cycles). Next, electrodeposition of $AuCl_4^-$ was used to generated the gold WE (6 mM $AuCl_4^-$ in 0.1 M KNO_3, -0.2 V, 800 s). Lastly, the gold WE was cleaned by cycling in acid (0.5 M H_2SO_4, -0.2 V to 1.35 V, 0.1 V/s, 20 cycles). All preparations for the gold WE were completed in a Teflon electrochemical cell using a Pt counter electrode and a Ag/AgCl reference electrode.[24,45]

Slip layer fabrication for the Esensor began by patterning Whatman 1 chromatography paper, outlining a T shape with black wax ink (Illustration 3a). Next the lower rectangle of the T shape was cut out to create a void space, and the chromatography paper was placed in an oven to melt the black wax through the paper (140 °C, 1 min). The Esensor was then assembled by aligning the slip layer over the base layer and folding the tab protruding from the base layer over the slip layer (Illustration 3a-c). Once assembled, the dimensions of the Esensor were 2.3 cm wide and 4.0 cm long with a 3 mm wide gold WE, a 1 mm wide counter electrode, and a 1mm wide Ag/AgCl reference electrode.

2.2.3 DNA Probe Immobilization

To aid in the immobilization of the DNA probe and electrochemical detection, the DNA probe was labeled with a thiol at the 5' end and a methylene blue molecule at the 3' end, respectively. The DNA probe sequence was as follows: 5'-HS-$(CH_2)_6$-ACTCTCGATCGGCGTTTTAGAGAGG-$(CH_2)_7$-NH-MB-3'.[46] The DNA probe immobilization followed protocols outlined by Plaxco and coworkers.[25] Briefly, the DNA probe was incubated with TCEP-HCl (10 mM, 1hr) to ensure the 5' thiol was reduced. Next, the DNA probe was resuspended in an optimum buffer (10 mM KH_2PO_4 and 500 mM NaCl, pH 7) to a final concentration of 500 nM and then incubated directly on the gold WE (20µL, 1 hr). After incubation, the gold WE was washed three times with water.

Finally, the electrode was blocked with 6-mercapto-1-hexonal (3 mM, 1 hr). The Esensor device, once modified, was either used immediately or dried using nitrogen and stored in a laminated pouch. The optimized probe density was 1.1 x 10^{12} molecules/cm^2 and was determined experimentally by maximizing the detection sensitivity.[26,47,48]

2.2.4 Esensor Detection of Complementary ssDNA Target

Once removed from the storage pouch, the slip layer of the Esensor was slipped down so the top cellulose region of the T shape aligns with the three electrodes (Illustration 4a). Buffer was dispensed through the sample application port to wet the chromatography paper, bringing the electrodes into electrochemical contact (20µL). A background scan was taken using alternating current voltammetry (ACV, -0.1 V - -0.38 V, 50 Hz, amplitude of 0.025 V) and then the slip layer was slipped up to its original starting position exposing the gold WE (Illustration 4b). A 20 µL aliquot of ssDNA target (target sequence: 5'-TAAAACGCCGATC-3') was incubated directly on the gold WE (1 nM-10 µM, 30 min) (Illustration 4c). After, the slip layer was slipped down once more and another ACV measurement was taken (Illustration 4d). Signal suppression was determined by comparing ACV measurements before and after ssDNA hybridization. To maximize signal suppression, target incubation time, probe density, and gold electrodeposition time were optimized following existing protocols.[26,45]

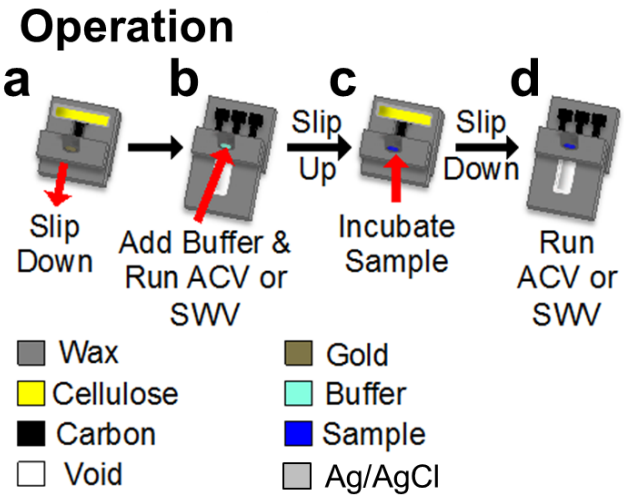

Illustration 4: Operation of the Esensor

a-b) The slip layer was slipped down and buffer was added to the at the sample injection port. A background ACV measurement was taken. c) The slip layer was returned to its original position to allow for direct incubation of the ssDNA target on the gold WE. d) After incubation, the slip layer was slipped down a final time, and a final ACV measurement was taken to determine the presence of ssDNA target analyte. Illustration 4 was adapted with permission from Ref. 1. Copyright 2014 American Chemical Society.

2.2.5 Esensor Specificity Experiment

Specificity experiments were performed following protocols outlined above in section 2.2.4; however, single, double and mismatch DNA targets were incubated directly on the gold WE instead of the complimentary ssDNA target following protocols outlined above. The following underlined nucleotide(s) identify the single, double, and mismatched DNA target sequences employed in the specificity tests: 5'-TAAAACTCCGATC-3', 5'-TAACACGCCGGTC-3', and 5'-ACGTGACATTTCT-3'.

2.2.6 Esensor Stability Experiment

Esensor probe stability was investigated by measuring signal suppression before and after drying. The gold WE was modified with the ssDNA probe, then dried using a stream of either (1) air or (2) nitrogen (10 min). ACV measurements were taken immediately after probe immobilization to determine the maximum background current. After drying with air or nitrogen, the probe was rehydrated by dispensing optimum buffer directly onto the gold WE (20 µL, 5 min). ACV measurements were taken again to determine if any loss in peak current had occurred.

2.3 Results and Discussion

2.3.1 Esensor Characterization

The topology of the gold WE was characterized via SEM (Figure 1). As seen in the SEM image, gold clusters were observed on the screen printed carbon electrode. The formation of the gold clusters was likely due to areas of different conductance within the carbon paste. The geometric area covered by gold clusters was calculated to be 58% using Image J software. The electroactive surface area was determined by integration of the gold reduction peak using cyclic voltammetry. The surface roughness, or ratio between electroactive surface area and geometric surface area, was calculated to be 2.17.[24]

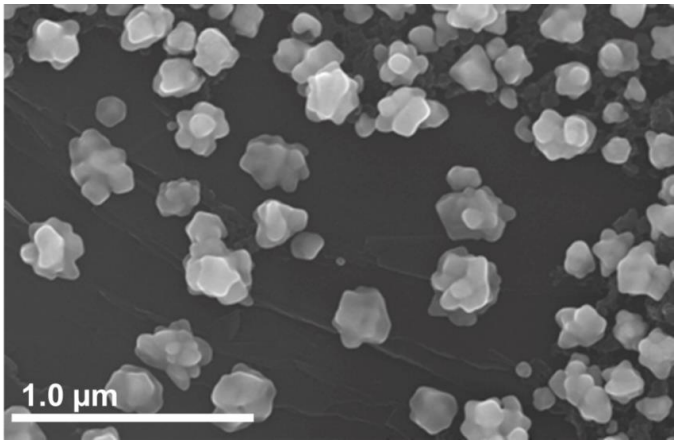

Figure 1: SEM Image of Esensor Gold Working Electrode

The dark gray background is the carbon paste electrode. The lighter gray clusters are gold clusters on the carbon electrode. The surface coverage of the gold clusters was 58% and the surface roughness ratio was 2.17. Reprinted with permission from Ref. 1. Copyright 2014 American Chemical Society.

2.3.2 Esensor Detection of Complementary ssDNA Target

As seen in Illustration 5, the DNA probe (25 nucleotides) has a stem-loop structure with a methylene blue redox label attached to the 3' end. Initially this molecule was close to the electrode surface permitting efficient electron transfer from the methylene blue to the electrode; however, upon ssDNA target (13 nucleotides) hybridization, the probe stem-loop structure unfolded. The unfolding moved the MB redox label further from the electrode surface, thereby prohibiting efficient electron transfer and reducing faradaic current.

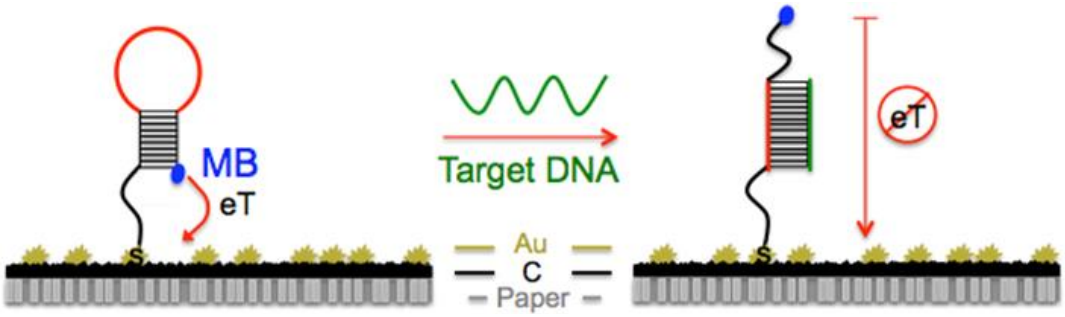

Illustration 5: Esensor Detection of ssDNA by DNA Probe – "Off" Sensor

The hybridization of the DNA target moved the methylene blue further from the gold WE, thereby preventing efficient electron transfer to the electrode. Signal was monitored using ACV. Reprinted with permission from Ref. 1. Copyright 2014 American Chemical Society.

The reduction in current resulting from ssDNA hybridization with the DNA probe was monitored using a potentiostat (Figure 2). The background current of the Esensor prior to hybridization was 0.95 µA. Hybridization with 10.0 µM complementary ssDNA strand resulted in a 45% reduction of peak current to 0.53 µA (Figure 2). The average signal suppression upon addition of 10 µM complementary ssDNA was 51% $\pm$ 5% as measured by five independently fabricated Esensor devices (Figure 3).

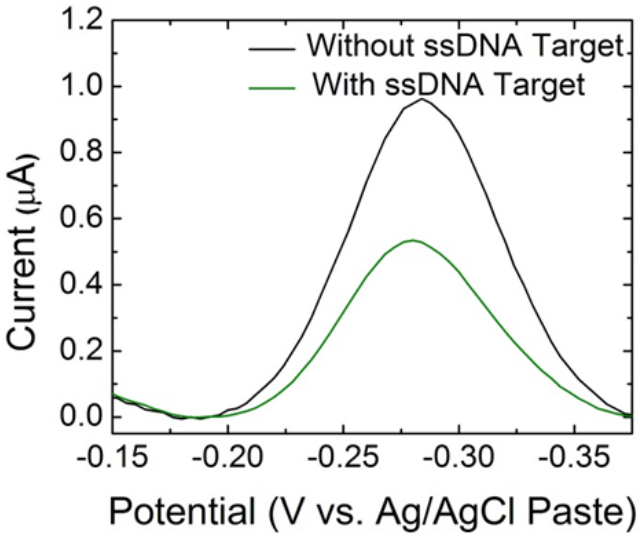

Figure 2: Detection of ssDNA Targets using the Esensor

Data acquired from an Esensor experiment. A drop in ACV measurement resulted from ssDNA hybridization with the DNA stem-loop probe. ACV measurement taken before ssDNA hybridization showed a maximum peak current of 0.95 µA (black trace). Addition of 10 µM ssDNA target resulted in a decrease in peak current to 0.53 µA (green trace). The signal was reduced by 45%. The data has been baseline subtracted. Reprinted with permission from Ref. 1. Copyright 2014 American Chemical Society.

2.3.3 Esensor Specificity

To determine the Esensor specificity, three ssDNA targets were tested. The first and second ssDNA targets contained one and two nucleotide mismatches with respect to the DNA probe, respectively. The third ssDNA target was entirely mismatched with respect to the DNA probe. The first and second mismatched ssDNA targets (10 µM) were incubated with the DNA probe and resulted in an 18 ± 5% and 14 ± 7% signal suppression, respectively (Figure 3). The entirely mismatched ssDNA target suppressed the signal by 4 ± 2%. Taken together, these data suggest that as the number of mismatched base pairs increases, the amount of signal suppression decreases. This

anticipated result was most likely due to the mismatched ssDNA targets' inability to hybridize and displace the methylene blue from the electrode surface.[27]

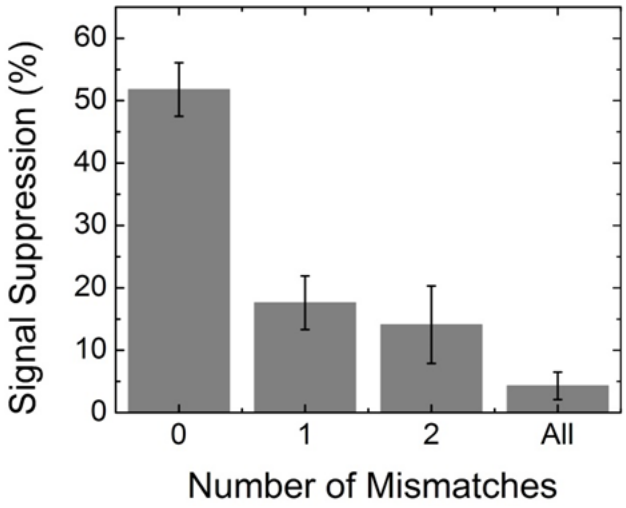

Figure 3: Detection of Mismatched ssDNA Targets

Histogram summarizing the signal suppression from increasing the number of DNA mismatches between the ssDNA target and the DNA stem-loop probe. As the number of DNA mismatches increased, the ability for the ssDNA target to displace the DNA stem-loop probe decreased. The inability to for the ssDNA target to hybridize with the DNA probe resulted in little signal suppression. Reprinted with permission from Ref. 1. Copyright 2014 American Chemical Society.

2.3.4 Esensor LOD

A dose-response curve was created from which the Esensor's LOD was determined (Figure 4). Various concentrations of complementary ssDNA (1 nM-10 µM) were incubated with the DNA probe then analyzed using ACV. The LOD of the Esensor was 30 nM for the complementary ssDNA target.[49] The LOD for the Esensor was approximately 10 fold higher than what Plaxco and colleges had calculated using a gold disk electrode (10 pM).[29] This difference in LOD was most likely due to the difference in

the electrodes used in the experiments where a gold disk electrode would allow for more sensitive signal detection.

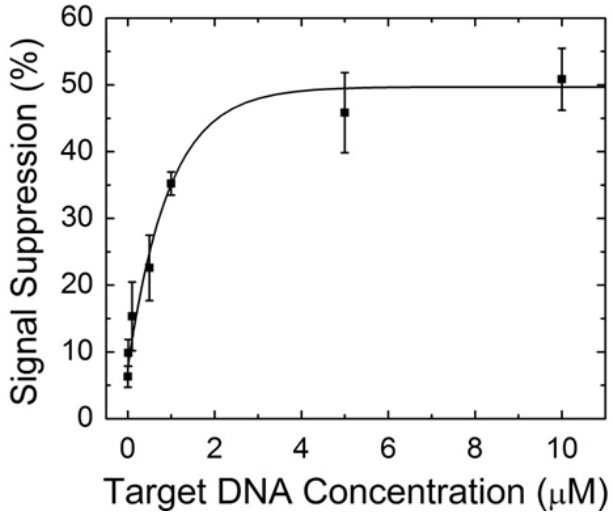

Figure 4: Dose-Response Curve

Esensor dose-response curve for complementary ssDNA target. The LOD of the Esensor was calculated to be 30 nM DNA. Experiments were performed in triplicate. Reprinted with permission from Ref. 1. Copyright 2014 American Chemical Society.

2.3.5 Esensor Stability

Storage of bio-reagents for sensing is challenging and many aptamer and DNA sensors must be kept in a solution or in a matrix of sugars and bovine serum albumin for storage prior to use.[25,47] Unfortunately, wax patterned paper is incompatible with such storage conditions, as it slowly absorbs liquid over time. For this reason, optimal storage conditions of the Esensor were tested. Briefly, ACV measurements were taken immediately after DNA probe immobilization. Next, the Esensor was dried using either air or nitrogen (Figure 5). Then, the DNA probes were rehydrated and a second ACV measurement was taken. Comparisons of ACV measurements before and after drying in

either air or nitrogen were used to determine optimal storage conditions. Optimal conditions would results in little to no change between the two ACV measurements. Esensors dried in air resulted in a peak current decrease of 39% (Figure 5a). This decrease in background current was likely due to oxidation of the DNA and alkanethiol monolayer.[50–52] Oxidation of DNA may cause the denaturation of the stem loop structure and/or cleavage of the DNA probe from the gold WE surface.[47] Alternatively, Esensors dried using nitrogen resulted in only a 3% decrease in peak current after rehydration (Figure 5b). Comparing the loss of signal due to storage conditions in air or nitrogen, 39% and 3% decrease, respectively, suggested drying sensors under nitrogen was optimal for long-term storage. Drying with nitrogen and storing in a sealed pouch for four weeks resulted in only a 6% loss in peak current (data not shown).

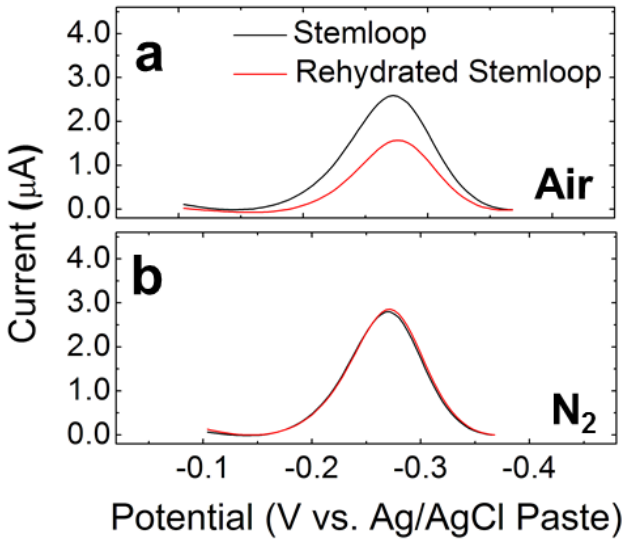

Figure 5: Peak Current Measurements After Rehydration

Alternating current voltammetry measurements of DNA probe before and after drying with (a) air and (b) nitrogen. Black traces represent the ACV measurement taken immediately after the immobilization of the stem-loop probe, and red traces represent the ACV measurement taken after rehydration of the stem-loop probe. From the data, Esensors dried using air were found to be unstable and resulted in a loss of activity, while Esensors dried using nitrogen retained activity. Reprinted with permission from Ref. 1. Copyright 2014 American Chemical Society.

2.4 Summary and Conclusion

In summary, we have created a PAD which employed target-induced conformational switching for quantitative electrochemical detection of ssDNA. The Esensor, an "off" sensor, showed an average signal suppression of 51% upon hybridization of 10 μM complementary ssDNA with a LOD of 30 nM. Furthermore, the Esensor was highly specific. Experiments employing single, double, and entirely mismatched ssDNA resulted in decreased signal suppression as expected: 18 ± 5%, 14 ± 7% and 4 ± 2%, respectively. Finally, optimal storage conditions for the Esensor were determined. Experiments showed Esensors dried using air were unstable and resulted in a

loss of activity, while Esensors dried using nitrogen retained activity. Furthermore, it was found that Esensors dried using nitrogen retained activity for up to 4 weeks.

This simple, robust sensor possessed several attractive features. One such feature was the SlipPAD[19] technology which imparts two key functionalities to the Esensor. First, the slip layer allows for timed incubation of samples directly on the gold WE. Secondly, the slip layer served to complete the circuit within Esensor, bringing the three electrodes into electrochemical contact. Another attractive property of the Esensor was the ease at which the user may reconfigure the sensor. The gold WE may be functionalized with any aptamer containing a free thiol functional group and redox label. This sensor could be easily reconfigured to detect a multitude of other biologically relevant molecules including RNA, hormones, environmental toxins, and proteins. Dr. Cunningham, the lead scientist for the Esensor project, went on to show the detection of thrombin using the Esensor platform.[1] Current focus of this sensor includes simultaneous detection of different analytes as well as detection of analytes in biologically relevant matrices. Results of such experiments will be reported in due course.

Chapter 3. Paper Fluidic Device for Rapid, Quantitative Electrochemical Detection of Bacteria

3.1 Introduction and Background

Bacterial detection is vital in industries ranging from healthcare to food preparation.[53,54] The World Health Organization (WHO) estimates that every year one in ten people worldwide contracts a foodborne illness and approximately 420,000 of these individuals die.[55] Three different pathogenic *Escherichia coli* (*E. coli*) outbreaks occurred in the US between October 2015 and March 2016 infecting 83 people and hospitalizing 27 people.[56–58] Outbreak prevention beings with early detection; however, once an outbreak occurs, rapid identification of the specific bacterial species responsible helps determine the medicinal treatment prescribed by doctors. This is especially important for patients with compromised immune systems. Moreover, identification of the specific bacterial species responsible for the outbreak reduces the use of broad-spectrum antibiotics that lead to proliferation of antibiotic-resistant bacterial strains.[59–61]

The primary methods used to detect, identify, and quantify bacteria are culturing, ELISA, and polymerase chain reaction (PCR) coupled to DNA detection.[53,62,63] These methods are slow, expensive, require specialized laboratory equipment and skilled personnel.[38,47] These limitations have led to the development of innovative biosensors that mitigate one or more of these factors.[62,64,65] Although these new bacterial sensors are promising, there are still many limitations and difficulties that require optimization for practical use such as quantitation, sensitivity, high cost, complex user operations, and the need for multiple reagents for bacterial detection. For example, Almeide and coworkers created a multiplexed lateral flow assay for detection of different species of bacteria via an immunosandwich assay.[54] This device used visual observation of highly concentrated AuNPs bound to bacteria to reveal their presence in a sample. This sensor was able to

detect bacteria in the range of 500-5,000 colony forming units per milliliter (CFU/mL), and had the additional benefit of not requiring preprocessing of biological samples. Albeit this sensor has addressed the limitations of cost and sample processing, it does not address the limitation of quantitation associated with colorimetric lateral flow devices.

To begin addressing the foregoing bacteria biosensor problems we have developed a PAD termed the oSlipB for quantitative electrochemical detection and identification of whole-cell bacteria (Illustartion 6). The device name, oSlipB, was derived from the following: "o" represents the origami fabrication method,[18] "Slip" indicates inclusion of a slip layer for assay control,[19] and "B" stands for bacteria. The oSlipB was the latest addition to the oSlip family of PADs developed by the Crooks group for the detection of biological analytes. These oSlip sensors have detected an array of analytes including a model analyte (biotin),[2] the protein TFF3 (a kidney disease marker),[3] ricin,[4] and a DNA oligomer characteristic of hepatitis B.[5] The use of hollow channels, a self-amplified electrochemical method and the fact that the oSlip sensors are easily reconfigurable have allowed them to become an extremely versatile sensor.

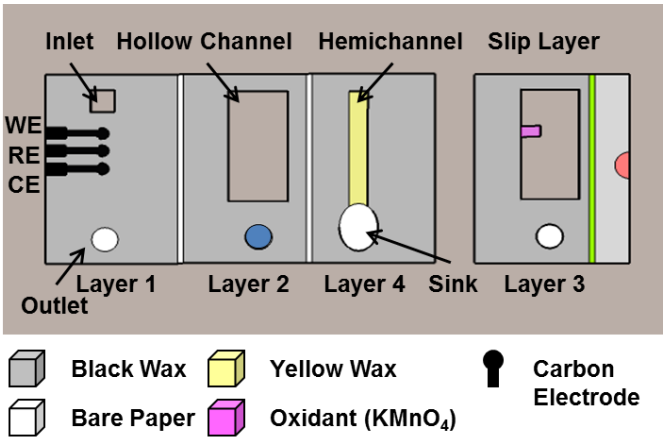

Illustration 6: Layout of oSlip

oSlip sensors are composed of four layers. The electrodes are located on layer 1. Once folded, the electrodes are located at the top of the hollow channel. The second layer forms the hollow channel and contains a dye to indicate cessation of solution flow. Layer 3, which contains the oxidizing agent, is inserted between layer 2 and layer 4. Layer 4 has a hydrophilic channel (hemichannel) and a sink that aid in the flow of solution through the device. Adapted from Ref. 4 with permission from The Royal Society of Chemistry.

There have been a few studies in which whole-cell bacteria have been detected using electrochemical methods similar to that reported here.[53,66,67] For example, Soltani and coworkers used commercial, disposable screen printed electrodes to detect bacteria via differential pulse anodic stripping voltammetry (ASV).[22] In this sensor, magnetic microbeads (MµBs) and AgNPs functionalized with anti-*Staphylococcus aureus* (*S. aureus*) aptamers were used to form a sandwich capture assay *in vitro*. After oxidation of the AgNPs using HNO_3, differential pulse ASV was used to determine the concentration of *S. aureus* in the sample. This sensor had a dynamic range of 1 x 10^1-1 x 10^6 CFU/mL and a LOD of 1 CFU/mL. While this bacterial detection method has addressed quantitation with high sensitivity it does not address the issues of cost, complex user operation, and the use of harsh reagents.

Here, we present the use of the oSlipB for quantitative electrochemical detection of *E. coli*. The oSlipB sensor employed antibody-functionalized MμBs and AgNPs to bind bacteria and form metalloimmunocomplexes (MCs). The MμBs were used to concentrate the MCs at the working electrode, and the AgNPs were employed for electrochemical detection of bacteria. This sensor used hollow channels, which minimized nonspecific adsorption within the paper device and allowed for transport of the large MCs within the sensor. Fluorescence microscopy, SEM, and TEM were employed to visualize the formation of MCs. The detection range and specificity of the oSlipB were determined electrochemically. At present, the lowest detectable concentration of bacteria was 1.3×10^7 cells/mL. Differentiation of bacterial species *E. coli*, *Bacillus subtilis*, and *Pseudomonas fluorescens* was possible due to the high specificity of antibody recognition. This sensor addressed the bacterial sensor limitations of time, user complexity, and cost. The total assay time was ~4 min, reagents were delivered via a slip layer, and the device fabrication was only $0.36 USD per assay including reagents.[5] The detectable concentration was too high for practical sensing applications, but we believe it will be possible to lower this value to a more desirable detection range in the near future.

3.2 EXPERIMENTAL

3.2.1 Chemicals and Materials

The following were provided by colleagues at UT-Austin: *E. coli* W3110 (Dr. Stephen Trent), *B. subtilis* and *P. fluorescens* (Dr. Adrian Keating-Clay), and the pGLO plasmid (Dr. Gene McDonald). *E. coli* serotypes O+K antibody, *E. coli* serotypes O+K antibody (biotin conjugate), and Dynabeads M-270 epoxy (2.8 μm) were purchased from ThermoFisher Scientific (Waltham, MA). Citrate-capped AgNPs (20 nm diameter) were

purchased from Ted Pella (Redding, CA). Carbon ink was purchased from Engineered Conductive Materials (Delaware, OH). The cylindrical neodymium magnet (N48, 1/16 in. x 1/2 in.) was purchased from Apex Magnets (Petersburg, WV). 1X phosphate-buffered saline (PBS) solution (10.0 mM phosphate, 138.0 mM NaCl, and 2.7 mM KCl, pH 7.4), $KMnO_4$, ampicillin sodium salt, Tween-20, Luria Bertani (LB) Broth, LB agar, and glycerol were all from Sigma-Aldrich (St. Louis, MO). Boric acid was from Merck (Darmstadt, Germany). Whatman grade 1 chromatography paper (180 μm thick), HCl, and NaOH were obtained from Fisher Scientific (Walthman, MA). All reagents were used as received without further purification. All solutions were prepared using deionized water (DI, >18.0 MΩ·cm) purified by a Milli-Q Gradient System (Bedford, MA) and performed at room temperature (23 ± 2°C).

3.2.2 oSlipB Device Fabrication and Assembly

The device fabrication procedure was adapted from previously reported protocols with some modifications.[2] Briefly, a pattern created using Corel Draw was printed onto a sheet of Whatman grade 1 chromatography paper using a Xerox ColorQube 8570DN wax printer. The printed devices were placed in an oven to melt the wax through paper (135 °C, 30 s). Black wax ink at 100% color saturation was used to impart maximum hydrophobicity to the chromatography paper while yellow wax ink at 60% color saturation was used to produce the hemichannel. The yellow wax ink at 60% color saturation melts through only ~50% of the chromatography paper thickness creating a thin hydrophilic cellulose channel to drive capillary flow. After cooling, the hollow channels were cut with a CO_2 laser cutter (Epilog Zing 16 Laser). Then, individual devices were separated from the original sheet of paper using the laser cutter. Next, thickened carbon ink (65 °C, 45 min, mixing every 10 min) was used to pattern stencil-

printed electrodes onto the paper devices. Thickened carbon ink was employed to prevent spreading of the ink under the stencil or on the paper device once the stencil was removed. Paper devices were baked in an oven to cure the carbon electrodes (65 °C, 1 h). The working, counter, and reference electrodes were all 2.0 mm in diameter. Each oSlipB was assembled by folding the device in an accordion fashion and inserting the slip layer between layers 2 and 4 (Figure 6a and 6b). Once folded each oSlipB was compressed between two acrylic plates and secured using binder clips (Figure 6c). The top acrylic plate had two holes drilled into it: one for the sample application port and the other to hold a small magnet over the WE. The electrodes protruded from the acrylic plates by 1 cm so they could be connected to a potentiostat (Figure 6c).

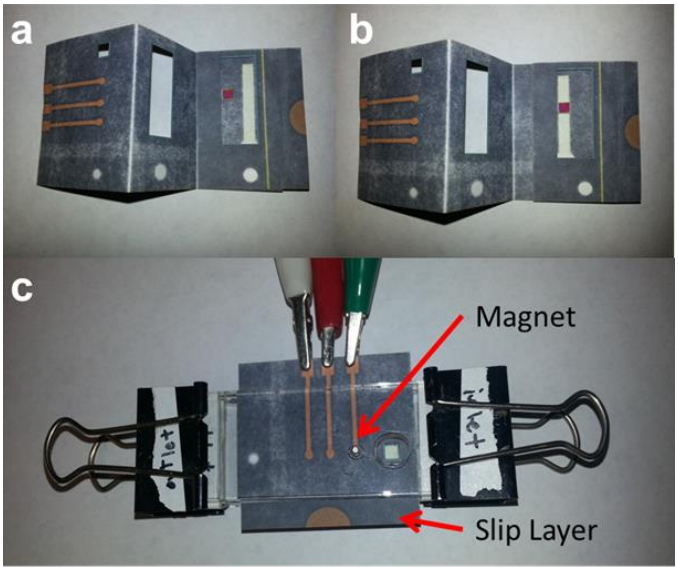

Figure 6: Photo of the oSlipB

(a) Photograph of an unfolded oSlipB. (b) Photograph of an unfolded oSlipB after the slip layer has been placed in the functional position. Note that the tab holding the oxidant (purple square) was positioned in the hollow channel in this configuration. (c) Photograph of an oSlipB sandwiched between two acrylic plates. The magnet, highlighted by the red arrow, can be seen above the WE and was held in place by a hole in the acrylic plates.

3.2.3 Functionalization of MµB with Antibodies

Antibodies were immobilized on epoxy-functionalized MµBs following a protocol provided by ThermoFisher. Briefly, MµBs suspended in dimethylformamide (DMF) were placed in a vial and held to a magnet (165 µL). The DMF was removed and the MµBs were resuspended in phosphate buffer (PB, 100 µL, 0.1 M, pH 7.4). Biotin conjugated *E. coli* serotypes O+K antibody in PB (100 µL, 1.0 mg/mL) and $(NH_4)_2SO_4$ (100 µL, 3.0 M) were added. The vial of MµBs was then incubated overnight with shaking using a Bioshake iQ (1400 rpm, at 37 °C, 18 hr). The next day the MµBs were washed a total of four times with 5% skim milk in 1X PBS. On the third wash the MµBs were placed in a shaker for blocking (1400 rpm, 1hr). The MµBs were stored in 5% skim milk in 1X PBS at 4 °C until needed.

3.2.4 Functionalization of AgNPs with Antibodies

The method for functionalizing AgNPs with antibodies was adapted from a method used to functionalize AgNPs with streptavidin.[68] First, citrate-capped AgNPs (1 mL, 5.6 x 10^{11} particles/mL) were thoroughly mixed with *E. coli* serotypes O+K antibody (25 µL, 1.0 mg/mL in 10 mM Tris, pH 8.0, 50 mM NaCl (T50)). Second, sodium bicarbonate was added to the vial, mixed thoroughly, and incubated on the bench top (10 µL, 1.0 M, 10 min). AgNPs were then mixed thoroughly with 2% PEG 6000 in DI H_2O (5 µL). Finally, the AgNPs were washed twice with 0.1% casein in T50 by centrifugation (16,600 x g, 18 °C, 20 min). After each wash the AgNPs were sonicated with a sonic probe tip to resuspend aggregated AgNPs. The functionalized AgNPs were then stored in 0.1% casein in T50 at 4 °C until needed.

3.2.5 Bacterial Growth and GFP Expression

E. coli W3110 was transformed with the pGLO plasmid by electroporation. Briefly, *E. coli* from a glycerol stock were first plated on LB agar and grown overnight (37 °C). The next day a single colony was picked and grown in LB broth to an OD_{600} = 0.7 (37 °C, 220 rpm). The *E. coli* were washed 3 times via centrifugation (4000 x g, 5 min) using 10% glycerol in DI H_2O with a volume of 10% of the original volume. The *E. coli* were resuspended in 10% glycerol in DI H_2O at 1% of the original volume and placed on ice. pGLO plasmid was mixed with the cells and incubated on ice (1 ng, 10 min). The *E. coli* were electroporated using a 1 mm electroporation cuvette with a Bio-RadGenePulser electroporater (1.8 kV, 200 ohms, and 25 µF). The *E. coli* were immediately resuspended in LB broth (800 µL) and grown at 37 °C for 1 hr. Finally, the *E. coli* were plated on ampicillin LB agar plates and grown overnight (37 °C). The next day a single colony harboring the pGLO plasmid was picked and grown in the presence of 0.2% arabinose to induce GFP expression.

For the calibration curve and specificity experiments, *E. coli*, *B. subtilis*, and *P. fluorescens* were grown separately in LB broth (37 °C, 220 rpm) until the desired OD_{600} was reached. Different concentrations of bacteria were made by dilutions using LB broth. OD_{600} measurements were obtained using a HP 8453 UV-vis spectrophotometer.

3.2.6 Ratio of *E. coli* to MµB

To determine the binding efficiency of the MµBs the following colony counting experiment was performed. First, MµBs were functionalized with anti-*E. coli* antibodies and blocked with casein (MµB-Ab). Two controls were prepared: (1) MµBs functionalized with casein only (cMµB) and (2) MµBs were omitted and only *E. coli* were present in the sample tube (*E. coli*). These two control experiments were used to estimate non-specific absorption of *E. coli* to the MµBs and the sample tubes,

respectively. *E. coli* (5.1 x 10^8 cells/mL) was incubated with antibody-functionalized MµBs or the controls in sample tubes for 10 min. The MµB-Ab sample and the two controls were washed by magnetic separation 15 times with 1X PBS containing 0.05% Tween-20 (v/v) (PBST). After washing, the concentration of MµBs in the MµB-Ab sample and controls were determined using a hemocytometer. Finally, the supernatant from the fifth, tenth, and fifteenth washes of the MµB-Ab sample and controls, along with the MµBs, MµB-Ab, and cMµB themselves, were plated separately and incubated overnight at 37 °C. The next day colonies were counted and the capture efficiency was calculated by dividing the number of colonies by the number of MµBs plated.

3.2.7 Formation of the Metalloimmunocomplex (MC)

To form the MC, antibody-functionalized MµBs were placed in a vial and held to a magnet (37.5 µL 830.2 fM). The storage solution (5.0% skim milk in 1X PBS) was removed and bacteria diluted in LB or in human urine (150 µL) were added to the vial. The vial was then inverted several times for mixing. Next, antibody-functionalized AgNPs were added to the vial and inverted several times for mixing (60 µL, 900 pM). The vial was then placed on a rotisserie rotator to form the MCs (10-30 min). The MCs were washed three times by magnetic separation (PBST, 300 µL) and resuspended in borate (300 µL, 0.1 M, pH 7.5).

3.2.8 SEM and TEM Preparation

All samples for SEM and TEM imaging were fixed using 0.25% glutaraldehyde in DI H_2O while mixing on a rotisserie mixer (45 min). Samples were then washed three times with DI H_2O. Lastly, samples were diluted to the desired concentration and aliquoted onto carbon TEM carbon grids (EMS400-Cu, Electron Microscopy Sciences). The SEM and TEM used were a Hitachi 5500-S and a FEI Tecnai, respectively.

3.2.9 Detection of MC in Conventional Electrochemical Cell

All electrochemical experiments were carried out using a CHI 627E potentiostat (CH Instrument, Inc., Austin, TX). The conventional electrochemical cell was a 2 mL Eppendorf tube (Figure 7), and the electrodes were: WE, 1.0 mm glassy carbon electrode (GCE); counter electrode, Pt wire; and reference electrode, Hg/Hg_2SO_4 (CH Instruments). MCs were formed using an *E. coli* concentration of 5.6 x 10^8 cells/mL. The experiment was carried out as follows. First, solution of borate (0.10 M) and NaCl (0.10 M, pH 7.5) was injected into an electrochemical cell (125 µL). Second, MCs (50 µL) and $KMnO_4$ were added to the electrochemical cell (50 µL, 200 µM). Third, a glassy carbon electrode was inserted into the solution and connected to the potentiostat as well as the reference and counter electrodes. Anodic stripping voltammetry was used in all electrochemical experiments (-0.7 V – 0.2V, 50 mV/s, 200 s deposition time).

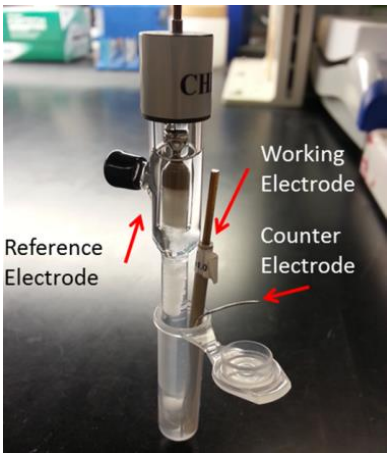

Figure 7: Photo of Conventional Electrochemical Cell

An Eppendorf vial was used as the conventional electrochemical cell. A 1.0 mm-diameter glassy carbon electrode, a Pt wire counter electrode, and a Hg/Hg_2SO_4 reference electrode were used for anodic stripping voltammetry experiments.

3.2.10 Detection of Bacteria in oSlipB

First, MCs formed in LB or in human urine were injected into the oSlipB (50 µL) (Illustration 8a). MCs introduced into the oSlipB flowed in their carrier solution through the hollow channel driven by the hydrophilic floor of the hemichannel (Illustration 8b). MCs were collected in the proximity of the WE by a magnet (Illustration 8c and 8d). This pre-concentration of the AgNPs at the WE was important for maximizing sensitivity and signal amplification.

A blue dye was pre-dispensed and dried on layer 2 of the oSlipB to indicate the cessation of solution flow in the channel (~15 s). Once the blue dye appears at the outlet of layer 1 the slip layer was used to introduce the pre-dried oxidant ($KMnO_4$) into the channel directly beneath the WE. The oxidant then diffused through the static solution toward the WE, where it oxidizes the AgNPs tethered to the bacteria that were captured by the MµBs (Illustration 8e). The resulting Ag^+ was then electrochemically reduced onto the WE electrode surface (Illustration 8f). This is the second form of signal amplification. Specifically, each 20 nm AgNP contains ~250,000 equiv. of electrons, which are harvested in the final ASV step of the assay (-0.7 V – 0.2V, 50 mV/s, 200 s deposition time) (Illustration 8g).[2] The resulting charge is directly related to the total number of bacteria originally present in the sample.

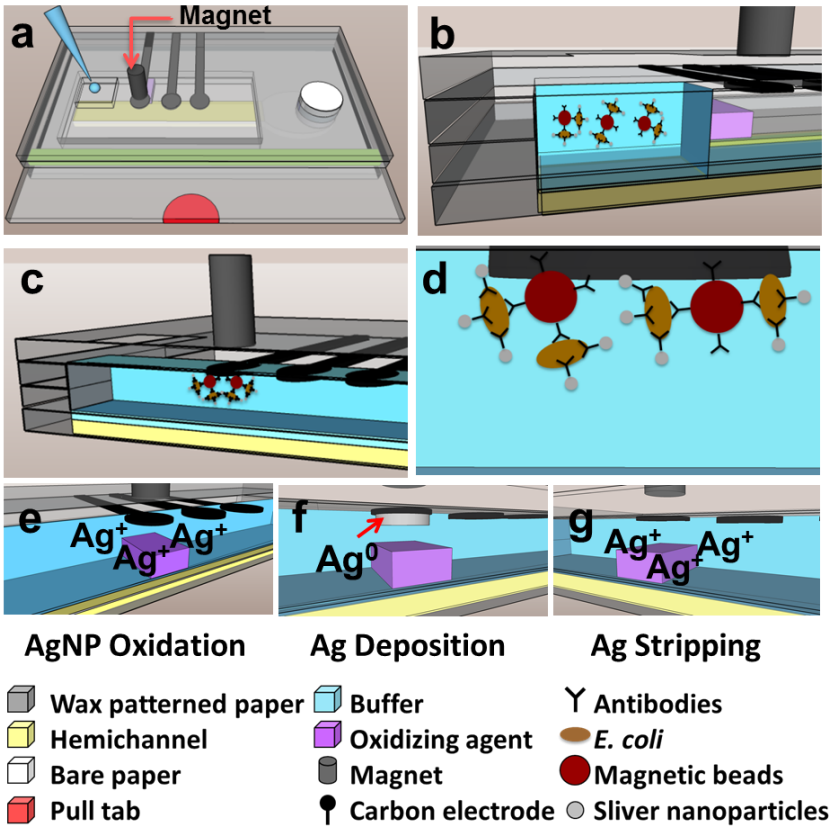

Illustration 7: Operation of oSlipB

a) MCs were formed in an Eppendorf tube and injected into the oSlipB. b) MCs then flowed down the hollow channel. c-d) MCs were captured at the WE by the magnet. e) $KMnO_4$ was introduced into the hollow channel, oxidizing the AgNPs. f-g) The Ag^+ ions were reduced onto the WE and then oxidized off to produce an electrochemical signal corresponding to the concentration of bacteria present. Adapted from Ref. 4 with permission from The Royal Society of Chemistry.

3.2.11 Oxidant Optimization

The optimum concentration of oxidant was determined by holding the concentration of *E. coli* constant (2.6 x 10^8 cells/mL) and varying the concertation of $KMnO_4$ used in the oSlipB. Different concentrations of $KMnO_4$ (1 µL, 14 mM-68.3 mM) were dispensed on the tab located on the slip layer. The oxidant was then dried using a

stream of nitrogen and the slip layer was inserted into the oSlipB. Electrochemical detection of *E. coli* in the oSlipB was carried out at each oxidant concentration.

3.2.12 Dose Response Curve in Buffer or Urine

A dose response curve for the oSlipB was created by varying the concentration of bacteria used to form MCs. *E. coli* was grown in LB to the desired concentration. MCs were formed as described above with dilutions of *E. coli* in buffer or urine (4×10^6 cells/mL to 4×10^8 cells/mL). The dose response curve obtained using MCs formed in buffer was made using standard ASV as described above. The dose response curve obtained using MCs formed in human urine was made using square wave ASV (-0.7 V – 0.2 V, step = 0.005 V, 25 Hz, amplitude = 0.05 V).

3.2.13 Specificity of oSlipB

Bacillus subtilis (B. subtilis) a Gram-positive bacteria and *Pseudomonas fluorescens (P. fluorescens)* a Gram-negative bacteria were used to determine the specificity of the oSlipB sensor. *E. coli, B. subtilis,* and *P. fluorescens* were grown separately in LB to desired concentrations. MCs were formed as described above using each bacterial species individually or with all three bacterial species mixed. MCs formed using an individual species had a concentration of 1.5×10^8 cells/mL. MCs formed in the presence of all three bacterial species contained 5×10^7 cells/mL for each species yielding a total bacterial cell concentration of 1.5×10^8 cells/mL.

3.3 Results and Discussion

3.3.1 *E. coli* are Responsible for MµB Aggregation

The minimum size of an *E. coli* (1 µm × 3 µm)[69] bound to a magnetic bead (2.8 µm in diameter) was calculated to be ~3.8 µm, but the actual size depends on the relative

orientation of the two objects. The multivalent nature of both the antibody-functionalized MµBs and the *E. coli* can result in crosslinking, thereby creating aggregates as large as 10-20 µm after just a few minutes of incubation. Two such aggregates were observed in an experiment where antibody-functionalized MµBs were incubated with *E. coli* in LB (Figure 8a). To determine if the *E. coli* were responsible for generating these larger complexes, an additional experiment was conducted where antibody-functionalized MµBs were incubated in buffer without *E. coli* (Figure 8b). The absence of aggregation observed in the later experiment suggests the multivalent bacteria were responsible for formation of the large ensembles. For the oSlipB sensor, this aggregation was not desirable but was an inevitable consequence of multivalency. Normal channels used in paper fluidic devices are filled with cellulose fibers have a particle-size cut-off of ~5 µm (unpublished data). With aggregates of 10-20 µm in diameter, hollow channels (~360 µm in height) were clearly essential.

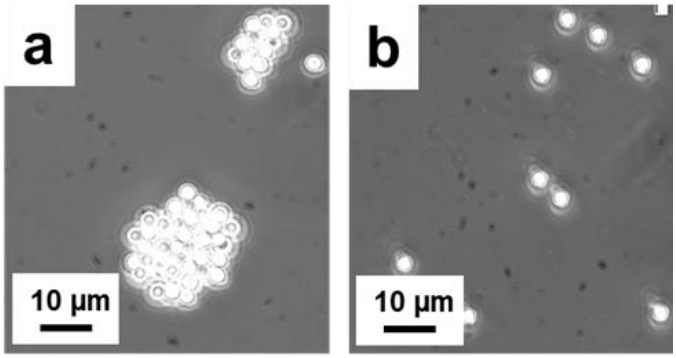

Figure 8: Micrographs Showing Aggregation of MCs

MCs were prepared by mixing antibody-functionalized MµBs with *E. coli* (5.6×10^8 cell/mL), adding antibody-functionalized AgNPs, incubating for 10 min, and then washing three times. a) Optical micrograph demonstrating the multivalent nature and corresponding aggregation of *E. coli* and MµBs. b) Optical micrograph illustrating the absence of MµB aggregation when *E. coli* were not present in the incubation mixture.

To further confirm that the multivalent bacteria were responsible for aggregation of the MµBs, a plasmid containing the gene for the green fluorescent protein (GFP)[70] was transformed into *E. coli*. The bacteria harboring the plasmid were cultured and the GFP protein was expressed. MµB/*E. coli* complexes were formed upon a 10 minute incubation of the fluorescent bacteria with MµBs and visualized using fluorescence microscopy. The micrograph showed a group of 23 ± 2 MµBs that appear as bright green spheres (Figure 9a). Theses MµBs were green in color and not white like in the previous figure due to the use of a GFP filter during image collection. The same sample was then illuminated with UV light to excite the GFP within the bacteria (Figure 9b). From the micrograph image, it was observed that 7 ± 1 *E. coli* cells were within the MµB cluster. The white oval in Figure 9a indicates the same *E. coli* highlighted by the white oval in Figure 9b. These micrographs confirm that the multivalent *E. coli* were responsible for MµB aggregation. Furthermore, these micrographs suggested that a MµB/*E. coli* aggregate contains a MµB:*E. coli* ratio of ~3:1.

To demonstrate how time effected aggregate formation, a sample was prepared as described above but samples were incubated overnight. Aggregates larger than 100 µm were observed using fluorescence microscopy (Figure 9c and 9d). Taken together, these results confirm that the *E. coli* was responsible for the ensemble formation, and the length of incubation time affected the diameter of these ensembles. From these data, an incubation time of 10-30 min was used for the oSlipB sensor assays.

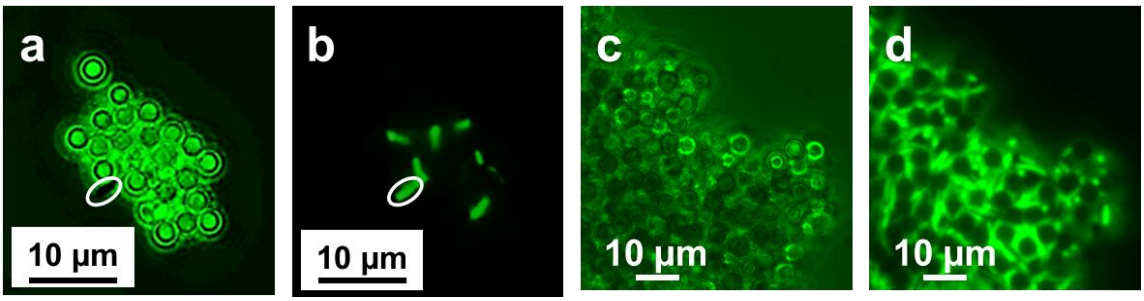

Figure 9: Fluorescence Micrographs Showing Aggregation of MCs

a) Fluorescent micrograph of a complex formed by MµBs binding to *E. coli* after a 10 min incubation. The white oval highlights an *E. coli* cell at the edge of the clustered of magnetic beads. A GFP filter and a white light source were used to obtain the micrograph. b) The exact same micrograph as (a) illuminated with UV light shows the presence of *E. coli* within the aggregated MµBs. The white oval indicates the same *E. coli* in both (a) and (b). c) Fluorescent micrograph of antibody-functionalized MµBs after an 18 h incubation with *E. coli* expressing GFP. d) The same micrograph as (c) illuminated with UV light shows the presence of a large number of *E. coli* within the MµB cluster.

3.3.2 MµB Bind *E. coli* at a ratio of 3:1

From the fluorescence microscopy experiments described above, it was estimated that the MµB to *E. coli* ratio was 3:1. To confirm this observation a colony counting experiment was performed to calculate the binding efficiency of the antibody-functionalized MµBs. Briefly, antibody-functionalized MµBs were mixed with *E. coli* in an Eppendorf tube for 10 min (MµB-Ab). The sample was then washed a total of 15 times. The supernatant containing unbound *E. coli* from washes 5, 10 and 15 were collected. Supernatant fractions and the extensively washed MµBs were plated on LB-agar and incubated overnight. The following day colonies were counted (Figure 10). Two controls were employed in this experiment. The first controlled for non-specific absorption of *E. coli* to MµB. This was accomplished by using casein blocked MµBs (cMµB) omitting antibody functionalization. The second control experiment tested for

non-specific absorption of *E. coli* onto the walls of the Eppendorf tubes. This was accomplished by omitting the addition of MµBs.

The appearance of relatively few colonies on the LB-agar plates from the washing fractions indicated that non-specific absorption was not a major concern when compared to the number of colonies captured by the MµBs functionalized with anti-*E. coli* antibodies (Figure 10). As expected, non-specific absorption decreased with more washing with nearly no *E. coli* remaining in the supernatant fraction of wash 15. From these experiments it was calculated that extensively washed MµBs functionalized with antibodies had a capture efficiency of ~3.2 ± 0.8 MµB/CFU. This result agreed with the ratio observed in the fluorescent experiments.

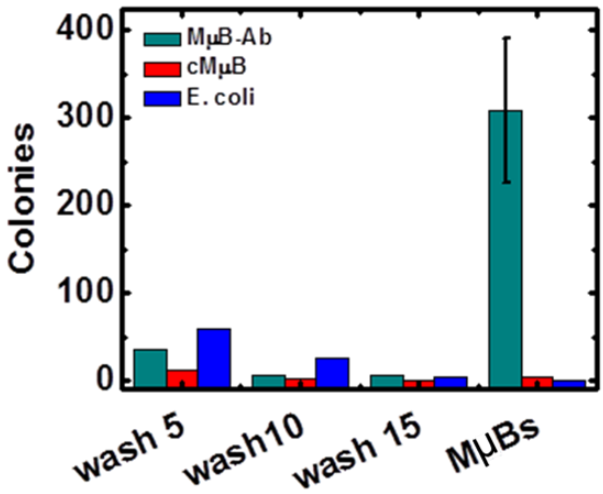

Figure 10: Histrogram of MµB capture efficiency

A histogram showing the average number of colonies present on the agar plates after overnight incubation at 37 °C. The last set of three columns, labeled MµBs, shows the number of bacterial colonies formed from plating the MµBs from the extensively washed sample (MµB-Ab) and one of the controls (cMµB). For the last control, (*E. coli*, blue) no MµBs were used; therefore, the supernatant after the fifteenth wash was plated. The MµB:*E. coli* ratio was calculated by dividing the number of beads plated by the CFU.

3.3.3 Characterization of Functionalized AgNPs

After the characterization of the MμB/*E. coli* ensemble we turned our attention to the AgNPs – the electrochemical signal component of the oSlipB sensor. Our sensor employed antibody-functionalized AgNPs. To confirm that the functionalization of the AgNPs was successful, stock citrate-capped AgNPs were compared to the antibody-functionalized AgNPs using TEM and UV-Vis. Briefly, stock citrate-capped AgNPs and functionalized AgNPs were washed in DI H_2O and aliquoted onto a TEM grid. As seen in the TEM micrograph below, some aggregation of AgNPs was observed for stock citrate-capped AgNPs whereas AgNPs functionalized with antibodies and blocked with casein showed no aggregation (Figure 11a-b, respectively).

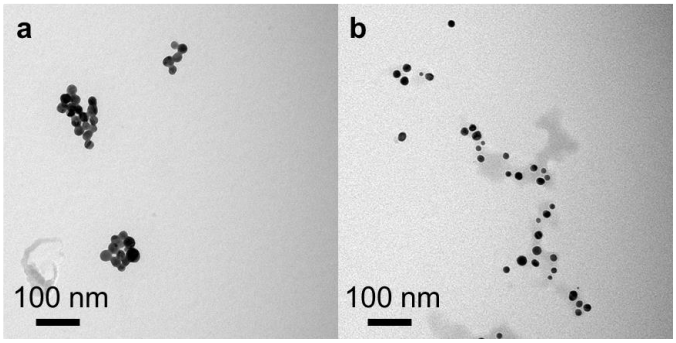

Figure 11: TEM of AgNPs

TEM micrographs of the AgNPs used in this project. a) A micrograph demonstrating the aggregation of stock citrate-capped AgNPs after being washed in DI water. b) A micrograph showing antibody-functionalized AgNPs remained soluble in DI water after washing.

UV-Vis spectrums obtained for the stock and functionalized AgNPs demonstrated the aggregation-shielding effects of absorbed proteins on the AgNPs in a high ionic strength solution (Figure 12). When stock citrate-capped AgNPs were incubated in PBS, a decrease in the silver plasmon peak indicated the AgNPs aggregated in the high salt

buffer (Figure 12). On the contrary, antibody-functionalized AgNPs showed no decrease in the sliver plasmon peak when suspended in water or PBS. The ability to remain soluble in high ionic strength solutions was desired, since many biological matrices contain high salt concentrations. Employing functionalized AgNPs that remain soluble in high salt would allow the oSlipB sensor to test for the presence of specific bacteria in many different biological matrices.

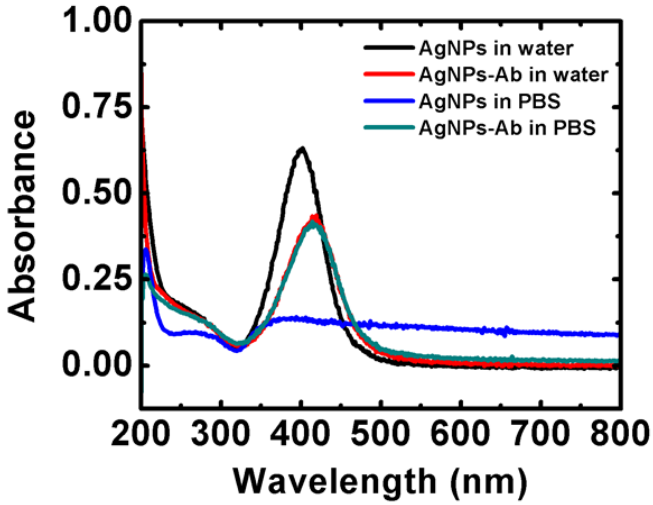

Figure 12: UV-Vis Spectra of Antibody Modified AgNPs

UV-Vis spectrum of citrate-capped AgNPs in water (black trace) The peak near 400 nm arises from the Ag plasmon absorbance. AgNPs modified with anti-*E. coli* antibodies in water (red trace) resulted in a peak shift from 400 nm to 410 nm. This shift was presumably due to the presence of antibodies and the blocking protein, casein, on the AgNPs. The absence of a well-defined plasmon peak suggests that the citrate-capped AgNPs aggregated in the high ionic strength solution (0.1 M PBS, blue trace); however the plasmon peak was retained in experiments using antibody-functionalized AgNPs incubated in PBS (green trace). Taken together, the data suggests that surface-bound proteins and antibodies prevented aggregation of AgNPs in high ionic strength solutions.

3.3.4 Antibody-Functionalized AgNPs Bind Surface of *E. coli*

Similar to the previous result, citrate-capped AgNPs incubated with *E. coli* in LB resulted with large AgNP aggregations on the surface of the bacteria (Figure 13a). Aggregation was likely a consequence of the diminished repulsive force between the citrate-capped AgNPs arising from the high ionic strength of the bacterial growth media.[71,72] Antibody-functionalized AgNPs blocked with casein and incubated with *E. coli* resulted in the presence of small aggregates, 3-15 AgNPs, (Figure 13b, red ovals) on the surface of the bacteria (Figure 13b, black arrow). As a control, casein-capped AgNPs incubated with *E. coli* showed no AgNP binding on the *E. coli* surface (Figure 13c). The lack of casein-capped AgNPs binding to the *E. coli* surface confirmed that the antibodies were responsible for binding of functionalized AgNPs to the surface of the *E. coli*.

The amount of AgNPs present on the surface of the bacteria directly relates to the electrochemical signal generated. It would appear that citrate-capped AgNPs would be ideal for bacterial detection; however, large AgNP aggregates on the bacteria surface would lead to an irreproducible correlation between signal generated and concentration of bacteria present in the sample. It is for this reason we employed antibody-functionalized AgNPs in the oSlipB sensor.

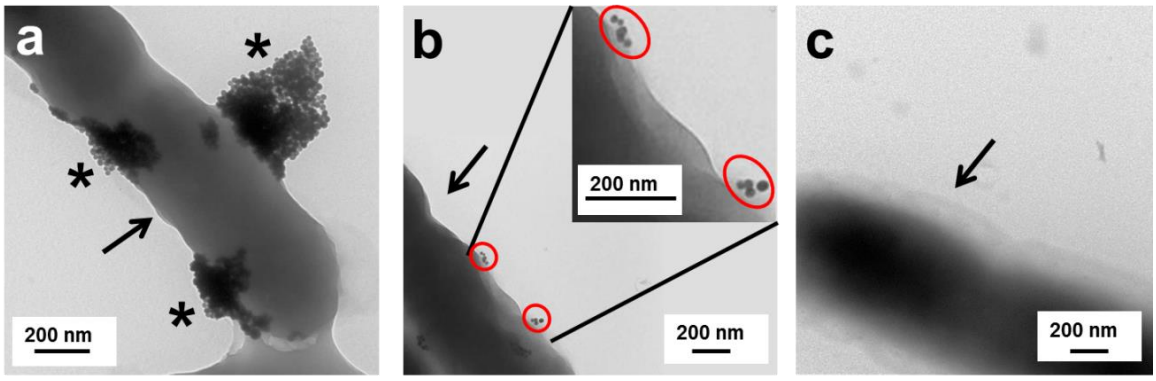

Figure 13: TEM of AgNPs on *E. coli*

Characterization of antibody-functionalized AgNPs binding to the surface of *E. coli*. *E. coli* and AgNPs were incubated for 10 min and washed before fixing for TEM imaging. a) TEM image of *E. coli* (black arrow) decorated with aggregated, citrate-capped AgNPs (black asterisks). b) TEM image of *E. coli* (black arrow) decorated with AgNPs (red ovals) that have been functionalized with anti-*E. coli* antibodies. c) TEM image of *E. coli* (black arrow) that have been incubated with casein-functionalized AgNPs. No AgNPs were observed bound to the surface, indicating that the antibody interactions were responsible for binding AgNPs to the bacterial surface, as expected.

3.3.5 Visualization of the Metalloimmunocomplex (MC)

To visualize the entire MC (MµBs, AgNPs, and *E. coli*) both the MµBs and AgNPs were functionalized with anti-*E. coli* antibodies and then incubated with *E. coli*. The resulting complexes were imaged by SEM (Figure 14a) and analyzed by energy-dispersive X-ray (EDX) spectroscopy (Figure 14b). The SEM image of the MC revealed small clusters of 3-30 AgNPs bound to the *E. coli* surface (Figure 14a). Furthermore, the SEM image confirmed that the *E. coli* bind to multiple MµBs within the MC (Figure 14a). The EDX scan, taken across the horizontal red line shown in Figure 14a, confirmed that the NPs observed within the MC were composed of Ag (Figure 14b). A large jump in percent composition of Ag corresponds to the exact location within the SEM image where AgNPs were located. Chloride was used as a control, because little to no chloride should be present in these samples (Figure 14b). Taken together, these experiments

confirmed the formation of the MC from MµBs, AgNPs and *E. coli*. Once we confirmed the formation of the MCs, we wanted to detect the electrochemical signal generated from the AgNPs within these MC complexes.

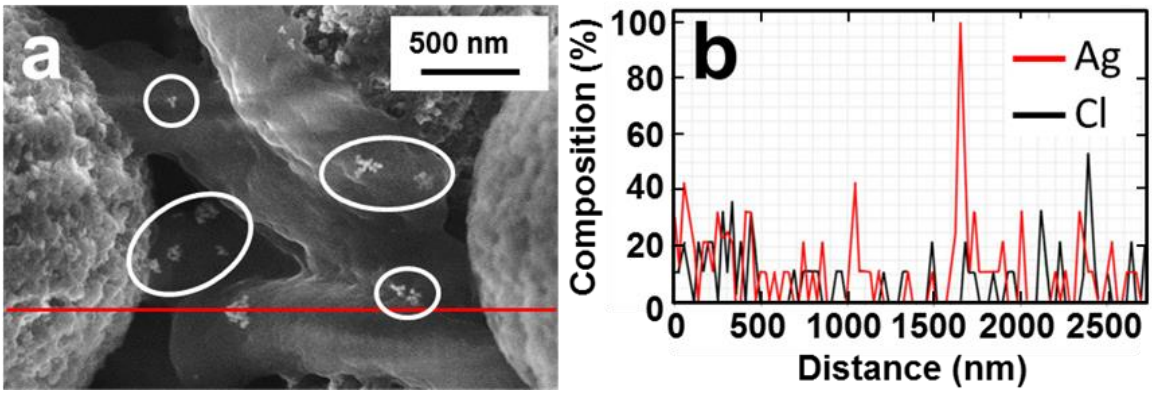

Figure 14: SEM and EDX of MCs

a) SEM image of the MC formed as described in the Experimental Section with a 10 min incubation. Small clusters of antibody-functionalized AgNPs are denoted by the white ovals bound on rod-shaped *E. coli*. Large spherical shapes on right and left of the image are MµBs. Red line is the EDX scan line. b) Plot showing the relative percentage of Ag (corresponding to the presence of AgNPs) and Cl^- in the SEM image denoted by the red line in (a). Cl^- is negative control. The Ag peak at ~1600 nm corresponds to presence of AgNPs in (a).

3.3.6 Electrochemical Detection of MC: Conventional Electrochemical Cell vs oSlipB Sensor

Before testing the oSlipB sensor, experiments were carried out in a conventional electrochemical cell to ensure that the assay chemistry functions as expected. MCs, $KMnO_4$ (oxidizing agent), and buffer were placed in an electrochemical cell. A glassy carbon, Pt wire and Hg/Hg_2SO_4 reference electrode were used to collect the data. The resulting Ag oxidation peaks for three independent replicate measurements were observed (Figure 15). The peaks are present at -0.240 ± 0.003 V and the average charge

under the current peaks is 1.84 ± 0.61 x 10^{-8} C. The reduction potential for Ag is 0.16 V vs. Hg/Hg_2SO_4, and the ~-400 mV shift from that value observed here was a consequence of 0.10 M Cl^- present in the electrolyte solution.[73] These experiments confirmed the assay chemistry functioned as expected.

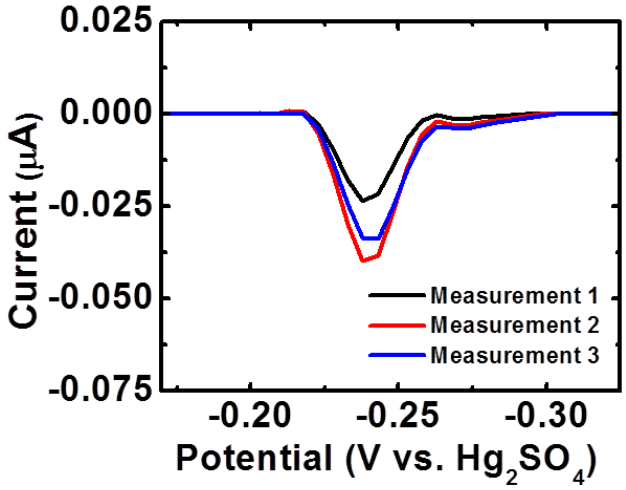

Figure 15: Electrochemical Detection of *E. coli* in Electrochemical Cell

All MCs were formed as described in the Experimental Section in LB broth and the incubation time was 10 min. ASV data obtained in the conventional electrochemical cell where each color represents an independent measurement. The peak potential is -0.240 ± 0.003 V and the average charge is 1.84 ± 0.61 x 10^{-8} C.

Next, the presence of bacteria in a sample was determined using the oSilpB sensor following protocols outlined in the Experimental Section (Section 3.2.10). The voltammograms obtained from the oSlipB sensor (Figure 16) were analogous to those obtained in a conventional electrochemical cell (Figure 15); however, there were obvious differences between the two data sets. One difference was that the charge measured for similar bacteria concentrations was ~35 times greater in the oSlipB compared to the conventional electrochemical cell. This large increase in signal was presumably due to

the following three factors. First, the oSlipB employed a magnet to concentrate MµBs (and hence the AgNPs) at the WE, whereas no magnet was employed in the conventional electrochemical cell experiments. Second, the flow of solution past the WE allowed a higher concentration of MCs to converge at the WE in the oSlipB than the conventional cell. Third, the hollow channel of the oSlipB was, in essence, a thin-layer cell,[73] and this resulted in less loss of Ag^+ into the bulk solution when compared to the conventional electrochemical cell.

Another difference between the data obtained in the conventional cell and the oSlipB is that the location of the ASV peak in the oSlipB is much less constant than in the electrochemical cell. This difference was a consequence of the different types of reference electrodes used in the two experiments. Specifically, a Hg/Hg_2SO_4 reference electrode was used in the conventional cell, whereas the oSlipB employed a carbon quasi reference electrode (CQRE). Unlike the Hg/Hg_2SO_4 reference electrode employed in the conventional cell, the potential of the CQRE varied due to its inconsistent makeup. In other words, variations in the carbon reference electrode and bulk solution led to varying peak potentials of the WE (Figure 16). Importantly, the exact location of the peak was not consequential as it can be easily integrated regardless of its position.

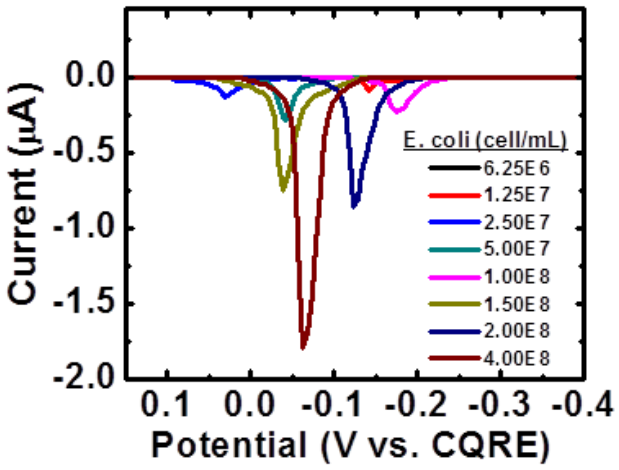

Figure 16: Electrochemical Detection of *E. coli* in the oSlipB

All MCs were formed as described in the Experimental Section in LB broth (10 min incubation). The concentrations of bacteria used to form the MCs are indicated in the legend. Charge increases with an increase in bacteria concentration.

3.3.7 Dose-Response Curve

Once the assay chemistry proved to function in the oSlipB, we sought to establish a dose-response curve. To obtain these data, MCs were formed in LB using a 15 min incubation time and an *E. coli* concentration range from 6.3 x 10^6-4.0 x 10^8 cells/mL. Plots of the ASV charge vs. *E. coli* concentration were obtained using the oSlipB (Figure 17). The linear range extends from 6.3 x 10^6 cells/mL to 2.0 x 10^8 cells/mL. The lowest detectable concentration was ~1.3 x 10^7 cells/mL with a charge of 2.12 ± 1.30 x 10^{-8} C. The best linear fit has an R^2 value of 0.98. The measurements were taken in triplicate and had an average coefficient of variance ~19%. The lowest concentration of *E. coli* had a coefficient of variance of ~61%. The oSlipB was able to quantitatively detect *E. coli*; however, the limit of detection and variance were too high for many practical applications.

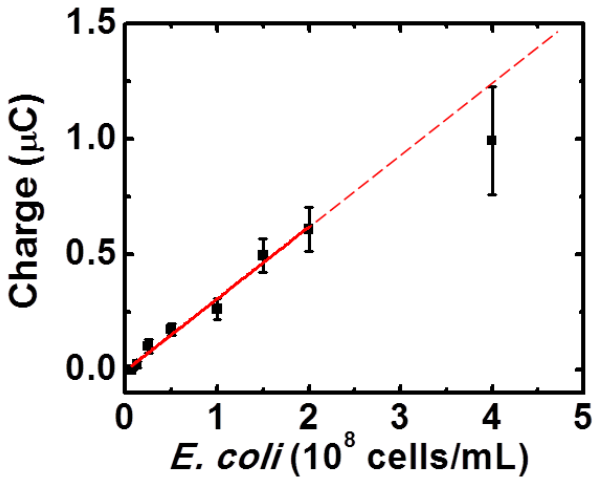

Figure 17: Dose-Response Curve in the oSlipB

All MCs were formed as described in the Experimental Section in LB broth (15 min incubation). The red line represents the best linear fit. The error bars represent the standard deviation from the mean for three independent ASV measurements using separate oSlipB devices. The lowest detected concentration of *E. coli* detected was 1.3 x 10^7 cells/mL.

3.3.8 Dose-Response Curve in a Biological Matrix

In a similar experiment, MCs were also formed in urine (15 min incubation). In an effort to lower the detection limit, square wave anodic stripping voltammetry was employed. This method allows for background signal suppression often leading to increased sensitivity.[73] With this detection method, the detectable *E. coli* concentration range in urine was 4.0 x 10^6 - 4.0 x 10^8 cells/mL. The lowest detectable concentration was 2 x 10^7 cells/mL with a charge of 7.00 ± 2.50 x 10^{-8} C (Figure 18). A slight hook effect can be seen at higher concentration of *E. coli* in urine (Figure 18). This may be explained by the high concentration of bacteria consuming too much oxidant, ultimately leading to a decreased signal. The average coefficient of variance in urine was ~28.5%. These results demonstrate the oSlipB was able to detect bacteria via formation of MCs in

human urine however; the lowest detectable concentration and variance were still too high for many practical applications.

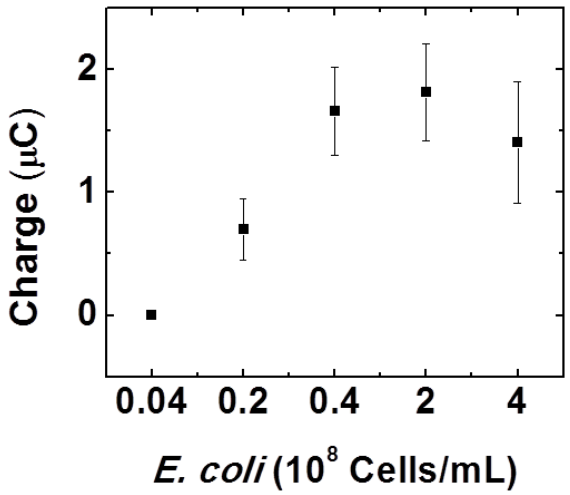

Figure 18: Electrochemical Detection of *E. coli* in Urine

A plot of charge vs. *E. coli* concentration gathered from MC formed in human urine. The error bars represent the standard deviation from the mean for three independent ASV measurements using separate oSlipB devices. The lowest detectable *E. coli* concentration was 2 x 10^7 cells/mL.

3.3.9 Importance of Oxidant Concentration for Bacterial Detection in oSlipB

We hypothesize that the suboptimal signal and coefficient of variance at lower *E. coli* concentrations was a consequence of the oxidant concentration relative to the *E. coli* concentration. Specifically, MnO_4^- can be reduced at the WE forming an insulating layer of MnO_2 over the surface of the WE.[2] At low *E. coli* concentrations this problem was exacerbated. Less oxidizing equivalents of MnO_4^- were consumed by the bacteria and AgNPs which allowed more MnO_4^- to be reduced on the WE. The formation of MnO_2 insulated the WE and impeded detection of *E. coli* (Figure 19a). Electrochemical detection of MCs in the oSlipB sensor was performed using concentration of MnO_4^-

ranging from 17-68 mM. A lower concentration of MnO_4^- allowed for the detection of lower *E. coli* concentrations (Figure 19a). To further demonstrate the effect of oxidant concentration on signal detection, an experiment was performed where the *E. coli* concentration was held constant and the MnO_4^- concentration was varied from 14-26 mM. Results from this experiment showed a narrow oxidant concentration was important for optimization of the oSlipB (Figure 19b). Both lower and higher concentrations of oxidant decreased signal. Taken together, the data from these experiments illustrate the importance of oxidant concentration relative to the bacteria concentration.

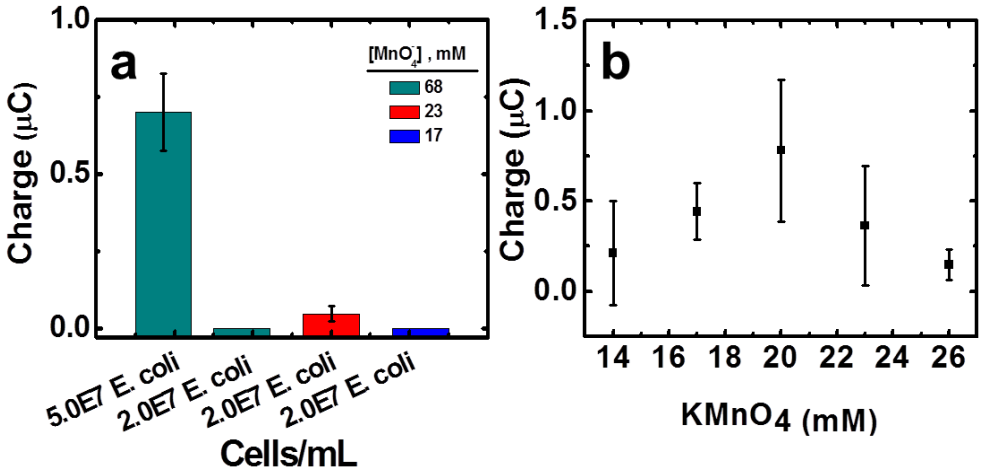

Figure 19: Oxidant Concentration Relative to *E. coli* Concentration

a) Histogram showing charge under the ASV peaks as a function of *E. coli* concentration for different concentrations of the oxidizing agent, MnO_4^-. The MC was formed as described in the Experimental Section (30 min incubation). The key result is that lower concentrations of MnO_4^- enabled a lower concentration of *E. coli* to be detected. When the analyte concentration was low relative the MnO_4^- concentration, the working electrode may become passivated by MnO_2 produced by the reduction of excess MnO_4^-. b) MCs were formed in LB (15 min incubation) using different concentrations of MnO_4^-. The *E. coli* concentration was held constant at 2.6 x 10^8 cells/mL and concentration of oxidant varied from 14-26 mM. The optimum MnO_4^- was 20 mM and both high and low concentrations of MnO_4^- resulted in a reduced signal when the *E. coli* was held constant.

3.3.10 oSlipB Specificity

To test the specificity of the oSlipB, AgNPs and MµBs were functionalized with anti-*E. coli* antibodies and incubated with *E. coli* alone or *E. coli* in the presence of *B. subtilis* (Gram-positive) and *P. fluorescens* (Gram-negative). In both experiments, the total concentration of bacteria present was 1.5×10^8 cells/mL. In the mixture experiment, the concentration of each bacterial species was 5×10^7 cells/mL. The resulting electrochemical charge measured from the *E. coli* alone was about three-fold higher than in the mixed bacteria experiment (Figure 20a). Additionally, when *E. coli* was present alone at the same concentration as in the mixture (5.0×10^7 cells/mL), the resulting charge was the same as in the mixed bacteria experiment. These results strongly suggest that the oSlipB was effective for distinguishing between multiple species of bacteria. (Figure 20a).

To determine if higher ASV signals could be obtained for lower *E. coli* concentrations, a longer incubation time (30 min vs. 15 min) was used to form MCs in the presence of each bacterial species alone or in the presences of all three species. The extended incubation time led to two- to three-fold enhancements in the signals for all samples containing *E. coli* (Figure 20b). As in the earlier specificity experiment when *E. coli* was present alone at the same concentration as in the mixture, the resulting charges were nearly the same (Figure 20b). No signal was obtained in experiments where the formation of MCs depended on the presence of *B. subtilis* or *P. fluorescens* alone (Figure 20b). Taken together, the data from the two specificity experiments confirm that the oSlipB was highly specific for *E. coli*, and that the magnitude of the ASV signal depended on the formation time of the MCs.

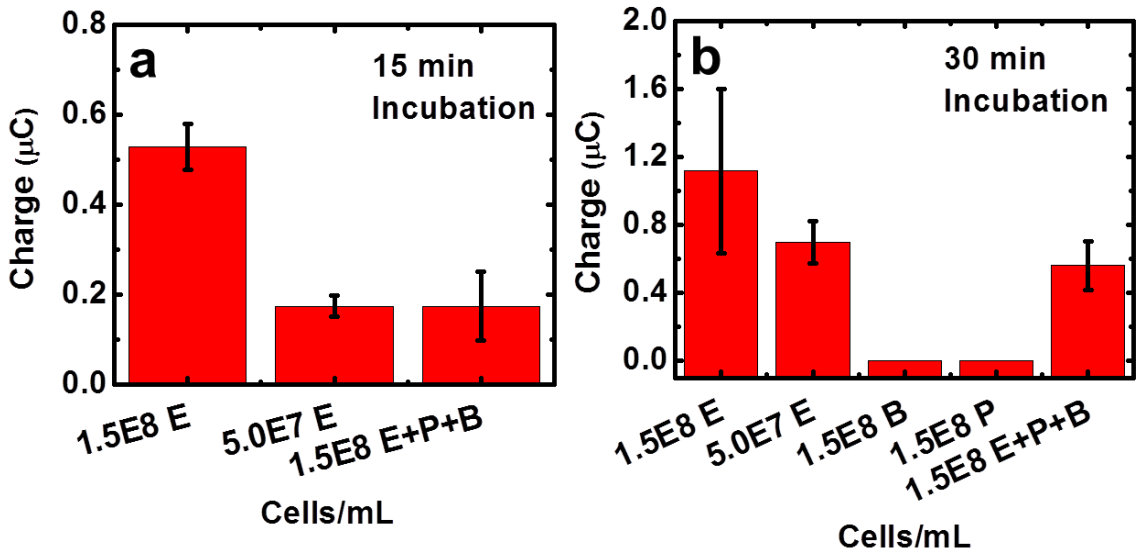

Figure 20: Specificity of oSlipB

Histograms showing how charge measured using the oSlipB depends on bacterial species. The MCs were formed as described in the Experimental Section using the incubation times indicated in the legends. The abbreviations for bacteria on the horizontal axes are: E = *E. coli*; B = *Bacillus subtilis*; and P = *Pseudomonas fluorescens*. a) Charge measured for MCs formed with *E. coli* alone or with all three bacterial species present (E+P+B). The MC incubation time was 15 min. The total cell concentration in the sample containing all three bacterial species was ~1.5 x 10^8 cells/mL with each species contributing 1/3 of the total concentration. b) Same as (a), but a 30 min MC incubation time.

3.4 Summary and Conclusions

Here, we have successfully shown that the oSlip sensor platform could be configured to sense specific species of bacteria. This new application complements earlier studies where the same device platform detected smaller biological molecules, e.g. proteins[4] and DNA[5]. Although the speed (~4 min, not including the off-chip incubation time), specificity, linearity, and cost (~$0.36 USD) of the oSlipB were highly appropriate for many sensor applications, the lowest bacterial concentration detected at 1.3 x 10^7 cells/mL was still too high for practical applications. We believe this high detection limit

was a result of several factors including aggregation of MCs, passivation of the WE by MnO_4^-, and potentially decreased affinity of the antibodies due to functionalization onto AgNPs. In the future our lab will focus on searching for an oxidizing agent that is compatible with paper and does not passivate the WE. Additionally, we intend to develop a better understanding of how the antibody-modified AgNPs interact with the surface of the bacteria. The ultimate goal for AgNP optimization would be to increase the number of AgNPs bound to the bacteria surface.

Even though the oSlipB has some limitations, this sensor illustrates many useful advantages over other bacterial sensors. First, the sandwich assay to form the MCs was performed in a single step, suggesting that multiple washing steps, and the additional on-chip complexity washing entails, may not be necessary. Ideally, however, the formation of MCs would be performed directly on the oSlipB. For this to occur, reagents would need to be pre-dispensed, stabilized, dried, and then resolvated at the time of need. Another advantage of the oSlipB over other bacterial sensors was that the capture component of the sensor allowed for relatively easy isolation of bacteria in complex matrices including urine and LB broth. We would like to test the oSlipB using other matrices such as ground water, food, and blood. Finally, we are working toward interfacing the oSlipB with a small, portable electronic reader that would provide a more realistic point-of-care test. Advances in all of these areas are underway and progress will be reported in due course.

Chapter 4. Overall Conclusion and Future Outlook

Work published by the Whitesides group in 2007 employing photoresist to pattern paper led many research groups to focus on the development of paper microfluidics, ultimately reinvigorating the PAD field.[9] The low cost and physical properties of paper combined with numerous detection method options available make paper based sensors an attractive platform for many applications ranging from clinical diagnostics to environmental monitoring.[6]

To that end, we have developed two paper-based sensors, the Esensor and the oSlipB, with point-of-care application in mind. These sensors have many attributes needed for point-of-care devices such as low cost, low power requirements, and ease of use. Additionally, the Esensor and oSlipB utilized many of the new technologies developed by the Crooks group including origami folding, the SlipPAD, and hollow channels. Both the Esensor and oSlipB devices employed electrochemical detection. This detection method offers many advantages over other detection methods such as sensitivity, selectivity, and easy integration with robust, miniaturized electronic devices.[7,12] While these sensors do not meet the necessary benchmarks for application yet, both contribute to a working body of knowledge for the development of affordable, portable health monitoring.

With the goal of health and environmental monitoring in mind, the WHO has established the acronym ASSURED for sensors intended for use in developing regions. ASSURED stands for: **A**ffordability, **S**ensitivity, **S**electivity, **U**ser-friendly, **R**apid and robust, **E**quipment free, and **D**eliverable.[6] While paper based sensors have the potential to fulfill all the requirements of ASSURED, many paper based sensors only partially fit the bill preventing their application. Some problems that still require further research include

reagent storage, stability, and resolvation. Furthermore, non-specific absorption and sample processing on paper sensors are challenges and warrant additional research.[13] A paper based sensor that has resolved many of the aforementioned problems and meets all the WHO requirements would surely be commercially successful, much like the home pregnancy test. Indeed, the fast paced research in the field of paper microfluidics and paper based sensors suggests that employment of paper sensors in many medical and environmental applications may soon become a reality.[13]

References

(1) Cunningham, J. C.; Brenes, N. J.; Crooks, R. M. Paper Electrochemical Device for Detection of DNA and Thrombin by Target-Induced Conformational Switching. *Anal. Chem.* **2014**, *86*, 6166–6170.

(2) Scida, K.; Cunningham, J. C.; Renault, C.; Richards, I.; Crooks, R. M. Simple, Sensitive, and Quantitative Electrochemical Detection Method for Paper Analytical Devices. *Anal. Chem.* **2014**, *86*, 6501–6507.

(3) DeGregory, P. R.; Tsai, Y.-J.; Scida, K.; Richards, I.; Crooks, R. M. Quantitative Electrochemical Metalloimmunoassay for TFF3 in Urine Using a Paper Analytical Device. *The Analyst* **2016**, *141*, 1734–1744.

(4) Cunningham, J. C.; Scida, K.; Kogan, M. R.; Wang, B.; Ellington, A. D.; Crooks, R. M. Paper Diagnostic Device for Quantitative Electrochemical Detection of Ricin at Picomolar Levels. *Lab Chip* **2015**, *15*, 3707–3715.

(5) Li, X.; Scida, K.; Crooks, R. M. Detection of Hepatitis B Virus DNA with a Paper Electrochemical Sensor. *Anal. Chem.* **2015**, *87*, 9009–9015.

(6) Nery, E. W.; Kubota, L. T. Sensing Approaches on Paper-Based Devices: A Review. *Anal. Bioanal. Chem.* **2013**, *405*, 7573–7595.

(7) Ahmed, S.; Bui, M.-P. N.; Abbas, A. Paper-Based Chemical and Biological Sensors: Engineering Aspects. *Biosens. Bioelectron.* **2016**, *77*, 249–263.

(8) Liu, H.; Xiang, Y.; Lu, Y.; Crooks, R. M. Aptamer-Based Origami Paper Analytical Device for Electrochemical Detection of Adenosine. *Angew. Chem. Int. Ed.* **2012**, *51*, 6925–6928.

(9) Martinez, A. W.; Phillips, S. T.; Butte, M. J.; Whitesides, G. M. Patterned Paper as a Platform for Inexpensive, Low-Volume, Portable Bioassays. *Angew. Chem. Int. Ed.* **2007**, *46*, 1318–1320.

(10) Martinez, A. W.; Phillips, S. T.; Whitesides, G. M. Three-Dimensional Microfluidic Devices Fabricated in Layered Paper and Tape. *Proc. Natl. Acad. Sci.* **2008**, *105*, 19606–19611.

(11) Yetisen, A. K.; Akram, M. S.; Lowe, C. R. Paper-Based Microfluidic Point-of-Care Diagnostic Devices. *Lab. Chip* **2013**, *13*, 2210.

(12) Cate, D. M.; Adkins, J. A.; Mettakoonpitak, J.; Henry, C. S. Recent Developments in Paper-Based Microfluidic Devices. *Anal. Chem.* **2015**, *87*, 19–41.

(13) Cunningham, J. C.; DeGregory, P. R.; Crooks, R. M. New Functionalities for Paper-Based Sensors Lead to Simplified User Operation, Lower Limits of Detection, and New Applications. *Annu. Rev. Anal. Chem.* **2016**, *9*, 183–202.

(14) Chen, G.-H.; Chen, W.-Y.; Yen, Y.-C.; Wang, C.-W.; Chang, H.-T.; Chen, C.-F. Detection of Mercury(II) Ions Using Colorimetric Gold Nanoparticles on Paper-Based Analytical Devices. *Anal. Chem.* **2014**, *86*, 6843–6849.

(15) CDC-Centers for Disease Control and Prevention. CDC - Malaria - About Malaria - Facts http://www.cdc.gov/malaria/about/facts.html (accessed Sep 12, 2016).

(16) Then, W. L.; Garnier, G. Paper Diagnostics in Biomedicine. *Rev. Anal. Chem.* **2013**, *32*.

(17) Fu, E.; Liang, T.; Spicar-Mihalic, P.; Houghtaling, J.; Ramachandran, S.; Yager, P. Two-Dimensional Paper Network Format That Enables Simple Multistep Assays for Use in Low-Resource Settings in the Context of Malaria Antigen Detection. *Anal. Chem.* **2012**, *84*, 4574–4579.

(18) Liu, H.; Crooks, R. M. Three-Dimensional Paper Microfluidic Devices Assembled Using the Principles of Origami. *J. Am. Chem. Soc.* **2011**, *133*, 17564–17566.

(19) Liu, H.; Li, X.; Crooks, R. M. Paper-Based SlipPAD for High-Throughput Chemical Sensing. *Anal. Chem.* **2013**, *85*, 4263–4267.

(20) Renault, C.; Li, X.; Fosdick, S. E.; Crooks, R. M. Hollow-Channel Paper Analytical Devices. *Anal. Chem.* **2013**, *85*, 7976–7979.

(21) Liana, D. D.; Raguse, B.; Gooding, J. J.; Chow, E. Recent Advances in Paper-Based Sensors. *Sensors* **2012**, *12*, 11505–11526.

(22) Abbaspour, A.; Norouz-Sarvestani, F.; Noori, A.; Soltani, N. Aptamer-Conjugated Silver Nanoparticles for Electrochemical Dual-Aptamer-Based Sandwich Detection of Staphylococcus Aureus. *Biosens. Bioelectron.* **2015**, *68*, 149–155.

(23) Jayasena, S. D. Aptamers: An Emerging Class of Molecules That Rival Antibodies in Diagnostics. *Clin. Chem.* **1999**, *45*, 1628–1650.

(24) Yang, W.; Gerasimov, J. Y.; Lai, R. Y. Folding-Based Electrochemical DNA Sensor Fabricated on a Gold-Plated Screen-Printed Carbon Electrode. *Chem. Commun.* **2009**, 2902.

(25) Xiao, Y.; Lai, R. Y.; Plaxco, K. W. Preparation of Electrode-Immobilized, Redox-Modified Oligonucleotides for Electrochemical DNA and Aptamer-Based Sensing. *Nat. Protoc.* **2007**, *2*, 2875–2880.

(26) White, R. J.; Phares, N.; Lubin, A. A.; Xiao, Y.; Plaxco, K. W. Optimization of Electrochemical Aptamer-Based Sensors via Optimization of Probe Packing Density and Surface Chemistry. *Langmuir* **2008**, *24*, 10513–10518.

(27) Xiao, Y.; Lou, X.; Uzawa, T.; Plakos, K. J. I.; Plaxco, K. W.; Soh, H. T. An Electrochemical Sensor for Single Nucleotide Polymorphism Detection in Serum Based on a Triple-Stem DNA Probe. *J. Am. Chem. Soc.* **2009**, *131*, 15311–15316.

(28) Xiao, Y.; Lubin, A. A.; Heeger, A. J.; Plaxco, K. W. Label-Free Electronic Detection of Thrombin in Blood Serum by Using an Aptamer-Based Sensor. *Angew. Chem. Int. Ed.* **2005**, *44*, 5456–5459.

(29) Fan, C.; Plaxco, K. W.; Heeger, A. J. Electrochemical Interrogation of Conformational Changes as a Reagentless Method for the Sequence-Specific Detection of DNA. *Proc. Natl. Acad. Sci.* **2003**, *100*, 9134–9137.

(30) Bonham, A. J.; Paden, N. G.; Ricci, F.; Plaxco, K. W. Detection of IP-10 Protein Marker in Undiluted Blood Serum via an Electrochemical E-DNA Scaffold Sensor. *The Analyst* **2013**, *138*, 5580.

(31) Ferguson, B. S.; Hoggarth, D. A.; Maliniak, D.; Ploense, K.; White, R. J.; Woodward, N.; Hsieh, K.; Bonham, A. J.; Eisenstein, M.; Kippin, T. E.; *et al.* Real-Time, Aptamer-Based Tracking of Circulating Therapeutic Agents in Living Animals. *Sci. Transl. Med.* **2013**, *5*, 1–9.

(32) Lai, R. Y.; Plaxco, K. W.; Heeger, A. J. Aptamer-Based Electrochemical Detection of Picomolar Platelet-Derived Growth Factor Directly in Blood Serum. *Anal. Chem.* **2007**, *79*, 229–233.

(33) Vallée-Bélisle, A.; Ricci, F.; Plaxco, K. W. Engineering Biosensors with Extended, Narrowed, or Arbitrarily Edited Dynamic Range. *J. Am. Chem. Soc.* **2012**, *134*, 2876–2879.

(34) White, R. J.; Kallewaard, H. M.; Hsieh, W.; Patterson, A. S.; Kasehagen, J. B.; Cash, K. J.; Uzawa, T.; Soh, H. T.; Plaxco, K. W. Wash-Free, Electrochemical Platform for the Quantitative, Multiplexed Detection of Specific Antibodies. *Anal. Chem.* **2012**, *84*, 1098–1103.

(35) Xia, F.; White, R. J.; Zuo, X.; Patterson, A.; Xiao, Y.; Kang, D.; Gong, X.; Plaxco, K. W.; Heeger, A. J. An Electrochemical Supersandwich Assay for Sensitive and Selective DNA Detection in Complex Matrices. *J. Am. Chem. Soc.* **2010**, *132*, 14346–14348.

(36) Swensen, J. S.; Xiao, Y.; Ferguson, B. S.; Lubin, A. A.; Lai, R. Y.; Heeger, A. J.; Plaxco, K. W.; Soh, H. T. Continuous, Real-Time Monitoring of Cocaine in Undiluted Blood Serum via a Microfluidic, Electrochemical Aptamer-Based Sensor. *J. Am. Chem. Soc.* **2009**, *131*, 4262–4266.

(37) Zuo, X.; Xiao, Y.; Plaxco, K. W. High Specificity, Electrochemical Sandwich Assays Based on Single Aptamer Sequences and Suitable for the Direct Detection of Small-Molecule Targets in Blood and Other Complex Matrices. *J. Am. Chem. Soc.* **2009**, *131*, 6944–6945.

(38) Lubin, A. A.; Lai, R. Y.; Baker, B. R.; Heeger, A. J.; Plaxco, K. W. Sequence-Specific, Electronic Detection of Oligonucleotides in Blood, Soil, and Foodstuffs with the Reagentless, Reusable E-DNA Sensor. *Anal. Chem.* **2006**, *78*, 5671–5677.

(39) Zuo, X.; Song, S.; Zhang, J.; Pan, D.; Wang, L.; Fan, C. A Target-Responsive Electrochemical Aptamer Switch (TREAS) for Reagentless Detection of Nanomolar ATP. *J. Am. Chem. Soc.* **2007**, *129*, 1042–1043.

(40) Li, X.; Qi, H.; Shen, L.; Gao, Q.; Zhang, C. Electrochemical Aptasensor for the Determination of Cocaine Incorporating Gold Nanoparticles Modification. *Electroanalysis* **2008**, *20*, 1475–1482.

(41) Lai, R. Y.; Walker, B.; Stormberg, K.; Zaitouna, A. J.; Yang, W. Electrochemical Techniques for Characterization of Stem-Loop Probe and Linear Probe-Based DNA Sensors. *Methods* **2013**, *64*, 267–275.

(42) Gerasimov, J. Y.; Schaefer, C. S.; Yang, W.; Grout, R. L.; Lai, R. Y. Development of an Electrochemical Insulin Sensor Based on the Insulin-Linked Polymorphicregion. *Biosens. Bioelectron.* **2013**, *42*, 62–68.

(43) Yang, Q.; Zhao, J.; Zhou, N.; Ye, Z.; Li, G. Electrochemical Sensing Telomere-Bending Motions Caused by hTRF1. *Biosens. Bioelectron.* **2011**, *26*, 2228–2231.

(44) Zhao, J.; He, X.; Bo, B.; Liu, X.; Yin, Y.; Li, G. A "signal-On" Electrochemical Aptasensor for Simultaneous Detection of Two Tumor Markers. *Biosens. Bioelectron.* **2012**, *34*, 249–252.

(45) Pereira, S. V.; Bertolino, F. A.; Fernández-Baldo, M. A.; Messina, G. A.; Salinas, E.; Sanz, M. I.; Raba, J. A Microfluidic Device Based on a Screen-Printed Carbon Electrode with Electrodeposited Gold Nanoparticles for the Detection of IgG Anti-Trypanosoma Cruzi Antibodies. *The Analyst* **2011**, *136*, 4745.

(46) Kang, D.; Vallée-Bélisle, A.; Porchetta, A.; Plaxco, K. W.; Ricci, F. Re-Engineering Electrochemical Biosensors To Narrow or Extend Their Useful Dynamic Range. *Angew. Chem. Int. Ed.* **2012**, *51*, 6717–6721.

(47) Lai, R. Y.; Seferos, D. S.; Heeger, A. J.; Bazan, G. C.; Plaxco, K. W. Comparison of the Signaling and Stability of Electrochemical DNA Sensors Fabricated from 6- or 11-Carbon Self-Assembled Monolayers †. *Langmuir* **2006**, *22*, 10796–10800.

(48) Ricci, F.; Lai, R. Y.; Heeger, A. J.; Plaxco, K. W.; Sumner, J. J. Effect of Molecular Crowding on the Response of an Electrochemical DNA Sensor. *Langmuir* **2007**, *23*, 6827–6834.

(49) Armbruster, D. A.; Pry, T. Limit of Blank, Limit of Detection and Limit of Quantitation. *Clin. Biochem. Rev.* **2008**, *29*, S49–S52.

(50) Jenner, A.; England, T. G.; Aruoma, O. I.; Halliwell, B. Measurement of Oxidative DNA Damage by Gas Chromatography–mass Spectrometry: Ethanethiol Prevents Artifactual Generation of Oxidized DNA Bases. *Biochem. J.* **1998**, *331*, 365–369.

(51) Li, Y.; Huang, J.; McIver, R. T.; Hemminger, J. C. Characterization of Thiol Self-Assembled Films by Laser Desorption Fourier Transform Mass Spectrometry. *J. Am. Chem. Soc.* **1992**, *114*, 2428–2432.

(52) Tarlov, M. J.; Newman, J. G. Static Secondary Ion Mass Spectrometry of Self-Assembled Alkanethiol Monolayers on Gold. *Langmuir* **1992**, *8*, 1398–1405.

(53) Freitas, M.; Viswanathan, S.; Nouws, H. P. A.; Oliveira, M. B. P. P.; Delerue-Matos, C. Iron Oxide/Gold Core/Shell Nanomagnetic Probes and CdS Biolabels for Amplified Electrochemical Immunosensing of Salmonella Typhimurium. *Biosens. Bioelectron.* **2014**, *51*, 195–200.

(54) Li, C.; Vandenberg, K.; Prabhulkar, S.; Zhu, X.; Schneper, L.; Methee, K.; Rosser, C. J.; Almeide, E. Paper Based Point-of-Care Testing Disc for Multiplex Whole Cell Bacteria Analysis. *Biosens. Bioelectron.* **2011**, *26*, 4342–4348.

(55) WHO | WHO's first ever global estimates of foodborne diseases find children under 5 account for almost one third of deaths http://www.who.int/mediacentre/news/releases/2015/foodborne-disease-estimates/en/ (accessed Jan 11, 2016).

(56) Escherichia coli O157:H7 Infections Linked to Costco Rotisserie Chicken Salad (Final Update) | November 2015 | E. coli | CDC http://www.cdc.gov/ecoli/2015/o157h7-11-15/index.html (accessed Dec 23, 2015).

(57) Escherichia coli O26 Infections Linked to Chipotle Mexican Grill Restaurants | November 2015 | E. coli | CDC http://www.cdc.gov/ecoli/2015/o26-11-15/index.html (accessed Dec 23, 2015).

(58) Escherichia coli O157 Infections Linked to Alfalfa Sprouts Produced by Jack & The Green Sprouts http://www.cdc.gov/ecoli/2016/o157-02-16/index.html (accessed Apr 5, 2016).

(59) Karasinski, J.; White, L.; Zhang, Y.; Wang, E.; Andreescu, S.; Sadik, O. A.; Lavine, B. K.; Vora, M. Detection and Identification of Bacteria Using Antibiotic Susceptibility and a Multi-Array Electrochemical Sensor with Pattern Recognition. *Biosens. Bioelectron.* **2007**, *22*, 2643–2649.

(60) Bootsma, M. C. J.; Diekmann, O.; Bonten, M. J. M. Controlling Methicillin-Resistant Staphylococcus Aureus: Quantifying the Effects of Interventions and Rapid Diagnostic Testing. *Proc. Natl. Acad. Sci. U. S. A.* **2006**, *103*, 5620–5625.

(61) Fluit, A. C.; Van Der Bruggen, J. T.; Aarestrup, F. M.; Verhoef, J.; Jansen, W. T. M. Priorities for Antibiotic Resistance Surveillance in Europe. *Clin. Microbiol. Infect.* **2006**, *12*, 410–417.

(62) Noble, R. T. A Review of Technologies for Rapid Detection of Bacteria in Recreational Waters. *J. Water Health* **2005**, *3*, 381–392.

(63) Hossain, S. M. Z.; Ozimok, C.; Sicard, C.; Aguirre, S. D.; Ali, M. M.; Li, Y.; Brennan, J. D. Multiplexed Paper Test Strip for Quantitative Bacterial Detection. *Anal. Bioanal. Chem.* **2012**, *403*, 1567–1576.

(64) Ahmed, A.; Rushworth, J. V.; Hirst, N. A.; Millner, P. A. Biosensors for Whole-Cell Bacterial Detection. *Clin. Microbiol. Rev.* **2014**, *27*, 631–646.

(65) Gracias, K. S.; McKillip, J. L. A Review of Conventional Detection and Enumeration Methods for Pathogenic Bacteria in Food. *Can. J. Microbiol.* **2004**, *50*, 883–890.

(66) Eksi, H.; Güzel, R.; Güven, B.; Boyaci, I. H.; Solak, A. O. Fabrication of an Electrochemical E. Coli Biosensor in Biowells Using Bimetallic Nanoparticle-Labelled Antibodies. *Electroanalysis* **2015**, *27*, 343–352.

(67) Zhang, X.; Geng, P.; Liu, H.; Teng, Y.; Liu, Y.; Wang, Q.; Zhang, W.; Jin, L.; Jiang, L. Development of an Electrochemical Immunoassay for Rapid Detection of E. Coli Using Anodic Stripping Voltammetry Based on Cu@Au Nanoparticles as Antibody Labels. *Biosens. Bioelectron.* **2009**, *24*, 2155–2159.

(68) Sönnichsen, C.; Reinhard, B. M.; Liphardt, J.; Alivisatos, A. P. A Molecular Ruler Based on Plasmon Coupling of Single Gold and Silver Nanoparticles. *Nat. Biotechnol.* **2005**, *23*, 741–745.

(69) Reshes, G.; Vanounou, S.; Fishov, I.; Feingold, M. Cell Shape Dynamics in Escherichia Coli. *Biophys. J.* **2008**, *94*, 251–264.

(70) Prasher, D. C.; Eckenrode, V. K.; Ward, W. W.; Prendergast, F. G.; Cormier, M. J. Primary Structure of the Aequorea Victoria Green-Fluorescent Protein. *Gene* **1992**, *111*, 229–233.

(71) Huynh, K. A.; Chen, K. L. Aggregation Kinetics of Citrate and Polyvinylpyrrolidone Coated Silver Nanoparticles in Monovalent and Divalent Electrolyte Solutions. *Environ. Sci. Technol.* **2011**, *45*, 5564–5571.

(72) nanoComposix · Silver Nanoparticles: Physical Properties http://nanocomposix.com/pages/silver-nanoparticles-physical-properties (accessed May 4, 2016).

(73) Bard, A.; Faulkner, L. *ELECTROCHEMCAL METHODS Fundamentals and Applications*; Second.; JOHN WILEY & SONS, INC., 2001.